

Research Paper

Downregulation of mitochondrial cyclooxygenase-2 inhibits the stemness of nasopharyngeal carcinoma by decreasing the activity of dynamin-related protein 1

Teng-Jian Zhou¹, Shi-Li Zhang¹, Cheng-Yong He¹, Qun-Ying Zhuang¹, Pei-Yu Han¹, Sheng-Wei Jiang¹, Huan Yao¹, Yi-Jun Huang², Wen-Hua Ling³, Yu-Chun Lin¹✉, Zhong-Ning Lin¹✉

1. State Key Laboratory of Molecular Vaccinology and Molecular Diagnostics, School of Public Health, Xiamen University, Xiamen Fujian 361102, PR China;
2. Zhongshan School of Medicine, Sun Yat-sen University, Guangzhou 510080, PR China;
3. Guangdong Provincial Key Laboratory of Food, Nutrition and Health, School of Public Health, Sun Yat-sen University, Guangzhou 510080, PR China.

✉ Corresponding authors: Y. Lin and Z. Lin, linych@xmu.edu.cn; linzhn@xmu.edu.cn. State Key Laboratory of Molecular Vaccinology and Molecular Diagnostics, School of Public Health, Xiamen University, Xiang'an south Road, Xiamen, 361102, China.

© Ivyspring International Publisher. This is an open access article distributed under the terms of the Creative Commons Attribution (CC BY-NC) license (<https://creativecommons.org/licenses/by-nc/4.0/>). See <http://ivyspring.com/terms> for full terms and conditions.

Received: 2016.09.20; Accepted: 2017.01.25; Published: 2017.03.23

Abstract

Cancer stem cells (CSCs) are a small subset of malignant cells, possessing stemness, with strong tumorigenic capability, conferring resistance to therapy and leading to the relapse of nasopharyngeal carcinoma (NPC). Our previous study suggested that cyclooxygenase-2 (COX-2) would be a novel target for the CSCs-like side population (SP) cells in NPC. In the present study, we further found that COX-2 maintained the stemness of NPC by enhancing the activity of mitochondrial dynamin-related protein 1 (Drp1), a mitochondrial fission mediator, by studying both sorted SP cells from NPC cell lines and gene expression analyses in NPC tissues. Using both overexpression and knockdown of COX-2, we demonstrated that the localization of COX-2 at mitochondria promotes the stemness of NPC by recruiting the mitochondrial translocation of p53, increasing the activity of Drp1 and inducing mitochondrial fission. Inhibition of the expression or the activity of Drp1 by siRNA or Mdivi-1 downregulates the stemness of NPC. The present study also found that inhibition of mitochondrial COX-2 with resveratrol (RSV), a natural phytochemical, increased the sensitivity of NPC to 5-fluorouracil (5-FU), a classical chemotherapy drug for NPC. The underlying mechanism is that RSV suppresses mitochondrial COX-2, thereby reducing NPC stemness by inhibiting Drp1 activity as demonstrated in both the *in vitro* and the *in vivo* studies. Taken together, the results of this study suggest that mitochondrial COX-2 is a potential theranostic target for the CSCs in NPC. Inhibition of mitochondrial COX-2 could be an attractive therapeutic option for the effective clinical treatment of therapy-resistant NPC.

Key words: mitochondrial cyclooxygenase-2, nasopharyngeal carcinoma, cancer stemness, dynamin-related protein 1, mitochondrial quality control.

Introduction

Nasopharyngeal carcinoma (NPC) is a malignancy with a remarkable geographic distribution. The incidence of NPC is particularly high in southern China (25-50 per 100,000 persons per year) [1]. Because the anatomic location is poorly accessible, treatment of NPC relies primarily on radiotherapy and chemotherapy [2]. Approximately 30% to 60% of NPC progress to a recurrent and resistant disease [3]. Many studies have reported that cancer stem cells (CSCs), possessing strong tumorigenic capability, may be responsible for this recurrence and resistance

of NPC [4-6]. Since the treatment of NPC is so inefficient, it is essential to identify novel targets for reducing the stemness of NPC so as to improve the outcome for patients [6].

Cyclooxygenase-2 (COX-2), encoded by the *PTGS2* gene, controls the synthesis of prostaglandin E-2 (PGE2). Since COX-2 plays a critical role in multiple processes, including cancer cell migration and invasion, and tumor-associated angiogenesis [7], increase in expression of COX-2 is recognized as a marker for the development and progression of

tumors [8]. One of our previous studies has revealed that COX-2 is a promising therapeutic target against NPC stemness [9], but it remains unknown how COX-2 enhances CSC stemness. A recent study reported that one of the cell organelles showing subcellular localization of COX-2 was the mitochondrion [7]. Another study showed that mitochondrial localization of COX-2 may confer to the resistance to apoptosis in several kinds of cancer, including hepatocellular carcinoma (HCC), colon cancer, and breast cancer [10]. The present study is aimed at characterizing the functional role of mitochondrial COX-2 in the stemness of NPC.

The mitochondrion is a double membrane-enveloped organelle that plays an essential role in all cells, including cell fates of cancers [11]. It has been identified as a new therapeutic target for eradicating CSCs, due to its critical role in the process of energy metabolism of CSCs [12-14]. The mitochondrion is highly dynamic, with its normal function maintained by continuous fusion and fission [15]. Mitochondrial fission plays a pivotal role in CSC stemness maintenance [16, 17]. Dynamin-related protein 1 (Drp1), a mitochondrial fission mediator encoded by the *DNM1L* gene, is a cytosolic GTPase [18]. Phosphorylation of Drp1 on Ser616 (p-Drp1^{Ser616}) enhances the activity of Drp1, whereas phosphorylation on Ser637 (p-Drp1^{Ser637}) represses its activity [17]. The activated form, p-Drp1^{Ser616}, has been closely linked to CSCs' biological characteristics and fate determination [17, 19]. Many lines of evidence show that Drp1 might be a promising target for controlling cancer stemness [17, 20]. A study from Shen et al. presented that the CSCs of NPC show a high rate of mitochondrial fission [14]. Considering that COX-2 is partly located at mitochondria, we hypothesized that COX-2 participates in the regulation of NPC stemness by increasing the activity of Drp1 and promoting mitochondrial fission.

In the present study, by analysing the gene expression in both tissues of NPC patients and fluorescently sorted CSCs from NPC cell lines by flow cytometry (FCM), we demonstrated that mitochondrial COX-2 increases the stemness of NPC by leading to the phosphorylation of Drp1 at serine 616. By both overexpression and knockdown of COX-2 or Drp1, we confirmed that mitochondrial COX-2 activates Drp1 by increasing the mitochondrial translocation of p53. We also found that resveratrol (RSV), a natural phytochemical which has been widely used for cancer chemoprevention [21], could suppress NPC stemness and sensitize NPC to 5-fluorouracil (5-FU), a classical chemotherapy drug for NPC, by inhibiting the mitochondrial COX-2/p-Drp1^{Ser616} pathway. Our findings provide

new insights for understanding mitochondrial COX-2 as a theranostic target and developing more effective therapeutic strategies for NPC treatment.

Materials and methods

Cell culture and reagents

Human NPC cell lines (CNE1 and CNE2) were from the Cancer Center of Sun Yat-sen University (Guangzhou, China). Cells are maintained in Dulbecco's Modified Eagle Medium (DMEM, Gibco, NY, USA) with 10% fetal bovine serum (FBS, Gibco, CA, USA) and 1% penicillin-streptomycin (Gibco) at 37°C in a 5% CO₂ humidified incubator (Thermo, CO, USA). Hoechst 33342, dimethyl sulfoxide (DMSO), verapamil, RSV, Mdivi-1, 5-FU were purchased from Sigma (MO, USA). Aspirin, celecoxib and indomethacin were purchased from Selleck (TX, USA).

Antibodies

The primary antibodies to Drp1, phospho-Drp1 (Ser616), p53, and cleaved-caspase 3 were purchased from Cell Signaling Technology (CST, MA, USA). Phospho-Drp1 (Ser637), ABCG2 (ATP-binding cassette sub-family G member 2), and Oct4 (octamer-binding transcription factor 4), ALDH1 (aldehyde dehydrogenase 1), and BAX (Bcl-2-associated X protein) antibodies were purchased from Ruiyingbio (Jiangsu, China). Mfn2 antibody was obtained from Abgent (NJ, USA). The antibody against β -actin was from Boster (Wuhan, China). The antibodies against COXIV, CD133, CD44, BMI1 (B lymphoma Mo-MLV insertion region 1 homolog), and Bcl-2 (B-cell lymphoma 2) were from Beyotime (Shanghai, China). LC3 antibody was purchased from Novus Biologicals (CO, USA). The peroxidase-conjugated affinitypure secondary antibodies goat anti-rabbit IgG and anti-mouse IgG were purchased from Thermo. Alexa Fluor[®] 488-labeled goat anti-rabbit IgG and DyLight[®] 405-labeled goat anti-mouse IgG were obtained from Beyotime.

Sorting and analysis of side population (SP) cells and main population (MP) cells

Following the method of our previous study [9], cells were digested with 0.25% trypsin-EDTA (Life, CA, USA) and adjusted to a concentration of 1×10⁶ cells/mL in DMEM supplemented with 2% FBS. Then the cells were incubated with 5 μ g/mL Hoechst 33342 alone or with 100 μ M verapamil at 37°C for 90 min in the dark with intermittent mixing. The cells were then washed twice with cold PBS supplemented with 2% FBS on ice. To make a single-cell suspension cells, cells filtered through a 40 μ m cell strainer (BD, CA,

USA), then the cells were analyzed and sorted on a MoFlo XDP cell Sorter (Beckman, CA, USA). The fluorescence of Hoechst 33342 was excited by the UV laser (355 nm), blue fluorescence was measured with a 450/20 BP optical filter and red fluorescence was measured with a 675 EFLP optical filter. The SP gate was defined as the diminished region in the presence of verapamil, a calcium ion tunnel antagonist-sensitive ABC transporter. The MP gate was defined as the region with high blue and red fluorescence. The ratios of SP and MP to total counted cells were recorded. SP and MP cells were collected for further experiments.

In vitro limiting dilution assay

To detect the frequency of CSCs in constructed cell lines, *in vitro* limiting dilution assays were performed according to Hu et al's method [22]. Briefly, 300, 250, 200, 150, 100, and 50 cells were seeded in six-well plates. At the end of ten days, the cells were washed by PBS, fixed in 4% paraformaldehyde (PFA), and stained with gentian violet for 15 min. The numbers of cells showing colony formation were counted. The frequency of CSCs was analyzed by extreme limiting dilution analysis (ELDA) software, available at <http://bioinf.wehi.edu.au/software/elda/>.

Quantitative real-time polymerase chain reaction (qRT-PCR)

Total RNA was extracted from SP and MP cells in CNE1 and CNE2 using Trizol reagent (Ambion, TX, USA) and reversely transcribed into complementary DNA with PrimeScript™ RT reagent kit (TaKaRa, Otsu, Japan) according to our previous study [9]. qRT-PCR was subsequently performed according to the manufacturer's instructions (TaKaRa, Otsu, Japan). The cycling conditions were 95°C for 30 s, 40 cycles of 95°C for 5 s and 60°C for 30 s. Expression levels of *ACTB* was used as an internal control. The relative expression levels of genes were displayed using the $2^{-\Delta\Delta C_t}$ method. The primer sequences used were listed in Table S1.

Mitochondrial morphological quantification

SP and MP cells sorted by FCM were cultured on coverslips overnight and loaded with 100 nM MitoTracker Red CMXRos (Life, CA, USA) in culture medium at 37°C for 30 min. Cells were fixed with 4% PFA for 45 min, and then observed immediately using a laser-scanning confocal microscope (Zeiss LSM780, Carl Zeiss, Jena, Germany). Using Rehman et al's methods [23], the mitochondrial fragmentation counts (MFC) were calculated to quantify changes in mitochondrial morphology. Continuous mitochondrial structures were imaged, counted with

the particle counting subroutine by ImageJ software (Bethesda, MD, USA), and normalized to the total mitochondrial area (in pixels). The number of mitochondrial fragments was counted by Image Pro-Plus software 6.0 (IPP 6.0, Media Cybernetics, MD, USA). $MFC = \text{Number of fragments} \times 10000 / \text{total mitochondrial area}$. The representative MFC values for ten randomly selected cells in each cell line were calculated and shown.

Gene expression analyses of NPC tissues in GEO database

Three public mRNA expression datasets including GDS3341, GDS3610 and GSE32389 were screened from Gene Expression Omnibus (GEO) database (<http://www.ncbi.nlm.nih.gov/geo/>). Table S2 lists the detailed information of these three datasets. The relative gene expressions of *PTGS2* (encoding gene for COX-2) and *DNM1L* (encoding gene for Drp1) in tumor tissues from NPC cohorts were analyzed as previously described [24]. Correlation between the expression of *PTGS2* and *DNM1L* was evaluated with Pearson's correlation analysis using the Statistical Package for Social Sciences (SPSS) version 16.0 (SPSS, IL, USA).

Establishment of stable *PTGS2*-overexpressing and -knockdown cell lines

The construction of stable *PTGS2*-overexpressing and -knockdown cell lines was previously described [9]. CNE1-*PTGS2* and CNE2-*PTGS2* cells were the *PTGS2*-overexpressing cell lines and CNE1-pBabe and CNE2-pBabe cells were the corresponding control cells. Similarly, CNE1-sh*PTGS2* and CNE2-sh*PTGS2* cells were the *PTGS2*-knockdown cell lines and CNE1-shCtrl and CNE2-shCtrl cells were the corresponding control cells.

Proximity ligation assay (PLA)

The protein interaction studies were performed with PLA. A Duolink® *In Situ* Detection Reagents (DUO92002, Sigma, MO, USA) was used according to the manufacturer's instructions. Briefly, cells were cultured on sterile coverslips in 24-well plates at a density of 5×10^4 cells per well overnight. After being fixed with 4% PFA and permeabilized using 0.5% triton X-100, cells were blocked in Duolink II solution for 1 h. The slides were incubated with anti-COX-2 antibody (1:200) or anti-p53 antibody (1:200) and anti-p-Drp1^{Ser616} antibody (1:400) at 4°C overnight, followed by incubation with Duolink PLA anti-Mouse PLUS and PLA anti-Rabbit PLUS proximity probes. After washing the slides three times, the ligation reaction was done for 30 min and the amplification was run for 100 min at 37°C. Then the slides were

visualized using a confocal microscope (Zeiss LSM 780). Images were analyzed with IPP 6.0 software.

siRNA transfection

Small interfering RNAs (siRNA) for *DNM1L* (si*DNM1L*) and *PTGS2* (si*PTGS2*), and a negative control (siNC), were obtained from Ribobio company (Guangzhou, China). Cells were seeded at close to 70% confluence in 6-well plates. For each well, 50 nM si*DNM1L*, si*PTGS2*, or siNC mixed gently with Lipofectamine 2000 (Life) was added to the cultured cells for 12 h.

Isolation of mitochondrial and cytosolic fractions

Mitochondrial and cytosolic fractions were prepared using a mitochondrial isolation kit (Enzo Life, PA, USA). Briefly, at least 5×10^7 cells of each group were harvested and washed twice with cold PBS, then centrifuged at $600 \times g$ at 4°C for 5 min. After resuspending the pellets in mitochondria isolation buffer and placing on the ice for 15 min, the mixtures were stirred with a whirlpool oscillator and centrifuged at $600 \times g$ for 10 min. The supernatants were collected and centrifuged at $12,000 \times g$ for another 10 min. The pellet was mitochondria and the supernatant was the cytosolic fraction. Resuspending the pellet in mitochondria lysate buffer and centrifuged at $12,000 \times g$ at 4°C for 10 min to achieve mitochondrial fractions. Proteins in both cytosolic and mitochondrial fractions were quantified with the bicinchoninic acid (BCA) protein assay and were used for western blotting (WB) analysis. COXIV and β -actin were used as loading controls for the mitochondrial (Mito) and cytosolic (Cyto) fractions, respectively.

Western blotting (WB) analysis

WB analysis was performed as described previously [24]. Briefly, cells were lysed in whole-cell lysate buffer containing 1% phosphatase inhibitor cocktail and NPC tumor tissues were lysed in RIPA buffer (Beyotime) with 1% phosphatase inhibitor cocktail. Mitochondrial and cytosolic fractions were prepared as described above. Lysates containing 20-30 μg protein were loaded onto 8% or 10% sodium dodecyl sulfate-polyacrylamide gels for electrophoresis (SDS-PAGE) and the separated proteins transferred to poly vinylidene fluoride (PVDF) membranes (Pall, NY, USA). After blocking with 5% fat free milk for 1 h in Tris-buffered saline (TBS), the membranes were incubated with the primary antibody overnight at 4°C and then with the peroxidase labelled secondary antibody for 1 h on the next day. WB bands were visualized with an enhanced chemiluminescence kit (Pierce, IL, USA). The blot intensities were analyzed by ImageJ software

and the relative expression values were calculated.

Co-localization in mitochondria

To study the co-localization of mitochondria and COX-2 or p53, cells were seeded on sterile coverslips in 12-well plates at a density of 1×10^5 cells per well. After loading cells with MitoTracker probe in culture medium at 37°C for 30 min, cells were fixed with 4% PFA for 45 min and permeabilized with 0.5% triton X-100 for 5 min. After blocking nonspecific binding with 1% bovine serum albumin (BSA), cells were treated with primary antibodies at suitable concentrations (COX-2, 1:200; p53, 1:200) overnight, followed with appropriate fluorescent secondary antibodies. Cells were then photographed with a laser-scanning confocal microscope (Zeiss). Three independent assays for each cell type were conducted and representative images are shown in the figures. The Manders' overlap coefficient [25] was used to measure the co-localization between mitochondria and COX-2 or p53. For each sample, the overlap coefficient for at least 10 cells was calculated with IPP 6.0.

MTT assay

Cells were seeded in 96-well plates at 8×10^3 cells/well. After cells attached, they were treated with various concentrations of 5-FU (0.125-80 μM) or 5-FU combined with RSV (100 μM), for 24 h. 20 μl MTT (5 mg/ml) was added to each well, incubated for 4 h, and supplemented with 150 μl DMSO to dissolve the resulting formazan. The optical density (OD) of each well was measured spectrophotometrically at 490 nm. The cell viability was calculated as following formula: Cell viability rate (%) = $(\text{OD}_{490\text{Sample}} - \text{OD}_{490\text{Blank}}) / (\text{OD}_{490\text{Ctrl}} - \text{OD}_{490\text{Blank}}) \times 100\%$. Each group was normalized to the untreated control cells.

Apoptosis assays

The Annexin V-FITC apoptosis detection kit (Beyotime) was used to identify apoptotic cells according to the manufacturer's instructions. After being treated with 5-FU (10 μM), RSV (100 μM), or 5-FU combined with RSV for 24 h, CNE1 and CNE2 cells were harvested and washed with PBS. The cell pellets were then resuspended in 195 μL Annexin V binding buffer and stained with 5 μL of Annexin V-FITC and 5 μL of propidium iodide (PI) for 20 min in the dark. The fluorescence was detected by FCM (Beckman, CA, USA). The data were analyzed using FlowJo v.7.6.5 (Tree Star Inc. Ashland, OR, USA).

In vivo xenograft mouse model

Six-weeks-old BALB/c nude mice were purchased from Slac Laboratory Animal Co. Ltd (Shanghai, China). A total of 1×10^7 CNE2 cell in 50 μl

PBS combined with 50 μ l of Matrigel (BD, CA, USA) were subcutaneously inoculated into the right flank of each mouse. When tumors reached palpable size (at day 14 after injection), mice were randomly divided into 4 groups of 6 mice each: physiological saline (Ctrl), 5-FU (2 mg/kg), RSV (50 mg/kg), or 5-FU combined with RSV. Every two days, the drugs were injected via tail vein and the tumor dimensions were measured using a digital caliper. The formula $(W^2 \times L)/2$ was used to estimate tumor volume, where L is the longer dimension and W is the shorter one. After five 2-day cycles of treatment, the mice were killed and tumors were excised and weighed. Tumor tissues were collected for subsequent western blotting or tissue sectioning and immunohistochemical analysis.

Immunohistochemical (IHC) analysis

The dissected tumor tissues were fixed in 4% PFA, paraffin embedded, and serially sectioned at 4 μ m thickness. Paraffin sections were deparaffinized with xylene and dehydrated with an ethanol series of increasing concentration. HE counter-staining was performed. IHC detection was accomplished with the UltraSensitive™ SP IHC Kit (MXB, Fuzhou, China) as in our previous study [24]. The primary antibodies were anti-COX-2 (1:250, Abcam), anti-p-Drp1^{Ser616} (1:200, CST), anti-ABCG2 (1:200, Ruiyingbio), and anti-Oct4 (1:200, Ruiyingbio). Quantitative analysis was performed with IPP 6.0.

Statistics

Unless otherwise indicated, all data shown are mean \pm standard deviation (SD) of at least three independent experiments. Statistical comparison of mean values in two groups was assessed using the Student's *t*-test in SPSS 16.0. Multiple groups were compared by one-way analysis of variance (ANOVA) with Dunnett's post-test. A *P* value of < 0.05 was considered to be statistically significant.

Results

Upregulation of COX-2 and Drp1 in the tumors of NPC patients and SP cells of NPC cell lines

In order to explore the functional role of COX-2 in the regulation of stemness of NPC, SP cells, which are considered to be a type of CSC [26], were sorted from CNE1 and CNE2 cells. The SP cells (the R2 gate) accounted for 1.72% and 3.03% of the total CNE1 and CNE2 cells, respectively. The main population (MP, represented the non-CSCs, the R3 gate) accounted for 48.18% and 38.23%, respectively (Fig. 1A). To verify

the stemness of SP cells, *in vitro* limiting dilution assay was performed using the SP and MP cells from NPC cells. The frequency of CSCs in CNE1-MP and CNE2-MP was 1/793.1 [95% confidence interval (CI) 1/898.8 to 1/699.9] and 1/580.9 (95% CI, 1/648.5 to 1/520.3), while CNE1-SP and CNE2-SP was 1/79 (95% CI, 1/86.2 to 1/72.4) and 1/58.7 (95% CI, 1/65.0 to 1/53.0). Compared with MP cells, SP cells showed more than a ten-fold increase in the frequency of CSCs (Fig. 1B). In addition, the mRNA and protein expression levels of COX-2, ABCG2, an important biomarker determining the SP cells' phenotype [27], Oct4, a marker for CSCs [28], and stemness-associated genes *NANOG*, *KLF4*, *BMI1* were significantly higher in SP cells than in MP cells (Fig. S1A). Some classical markers of NPC-CSC, including CD133, CD44, ALDH1 and BMI1, were higher in SP cells than in MP cells (Fig. S1B). Interestingly, we found, through MitoTracker Red staining and imaging with a confocal microscope, that mitochondria in SP cells were more fragmented and less elongated than in MP cells (Fig. 1C). WB analysis showed that the level of COX-2, ABCG2 and Oct4 in SP cells was higher than in MP cells. The expression level of total Drp1 (t-Drp1) did not show any significant difference between SP and MP cells. However, SP cells had both strikingly elevated phosphorylation of Drp1 at Ser616 (p-Drp1^{Ser616}) and less p-Drp1^{Ser637}, compared to MP cells. Mitofusin-2 (*Mfn2*), required for the fusion of mitochondria [29], was also downregulated in SP cells (Fig. 1D). Since the SP cells contribute to the radio-resistance of NPC tumors, we analyzed the relative expression levels of *DNM1L* (encoding Drp1) and *MFN2* (encoding Mfn2) in the cohort of radio-sensitive and -resistant NPC patients tissues available from the GEO database. We found that radio-resistant NPC tumors possessed high *DNM1L* and low *MFN2* expressions compared with radio-sensitive tumors (Fig. S2). Moreover, we have investigated the mRNA level of *PTGS2* (encoding COX-2) and *DNM1L* in a GEO cohort of NPC patients. Compared with normal nasopharyngeal epithelial tissues, the NPC tumor tissues exhibited relatively high *PTGS2* and somewhat elevated *DNM1L* expression (Fig. 1E, Fig. S3A). The expression of *DNM1L* was significantly correlated with *PTGS2* expression in these clinical samples (Fig. 1F, Fig. S3B). Our previous study showed that COX-2 could enhance the stemness of NPC [9], the present study confirmed that COX-2 is a promising therapeutic target for NPC and further hinted that the activation of Drp1 may be involved in the promotion of cancer stemness induced by COX-2.

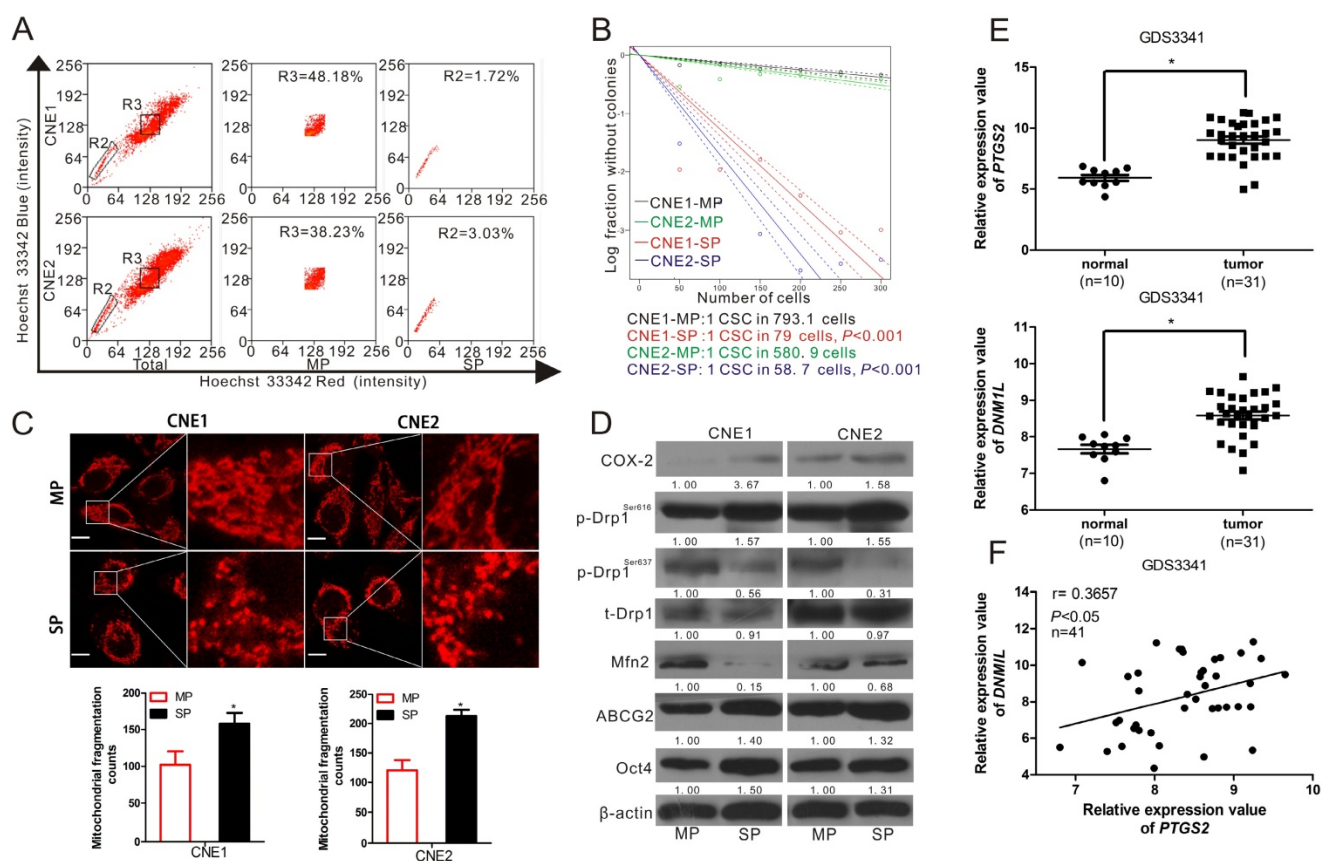


Figure 1. COX-2 and Drp1 were upregulated in the CSCs of NPC cells and NPC tissues. (A) Sorting SP and MP cells from CNE1 and CNE2 following Hoechst 33342 staining. A representative sample is displayed. The R2 gate shows the SP cells and R3 shows the MP cells. The percentages of SP cells in CNE 1 and CNE2 were 1.72% and 3.03%. (B) *In vitro* extreme limiting dilution assays to demonstrate the frequency of CSCs in SP and MP cells. The dashed lines show 95% confidence interval (CI) of the frequency of CSCs. (C) SP and MP cells were sorted by flow cytometry (FCM) and seeded on coverslips overnight. Mitochondria were stained by MitoTracker and imaged by confocal microscopy. Mitochondrial fragmentation counts were measured in 10 cells in each cell line of 3 independent experiments with IPP 6.0 ($\times 630$ magnification; scale bar, 10 μ m) and shown in lower bar graph. * $P < 0.05$ as compared with MP cells. (D) SP and MP cell lysates were analyzed by WB. Expressions of COX-2, p-Drp1^{Ser616}, p-Drp1^{Ser637}, total Drp1 (t-Drp1), Mfn2, ABCG2, and Oct4 were measured. * $P < 0.05$ as compared with MP cells. (E) PTGS2 and DNMT1 expression levels in one cohort of NPC patients are shown by scatter plots. The relative expression values were obtained from NCBI, GEO database (Accession No. GDS3341). The horizontal lines represent the median values (* $P < 0.05$). (F) The correlation between the expression of PTGS2 and DNMT1 was calculated by Pearson's correlation analysis.

Overexpression of COX-2 increases the interaction of COX-2 with p-Drp1^{Ser616} and the stemness of NPC

To determine the relationship of Drp1 and COX-2, the overexpression of COX-2 was established in CNE1 and CNE2 cell lines. Immunofluorescence analysis revealed that COX-2 overexpression increased the proportion of fragmented mitochondria. The level of COX-2 localization in mitochondria was increased in both CNE1-PTGS2 and CNE2-PTGS2 cells (Fig. 2A). PLA assays showed that COX-2 overexpression significantly enhances the interaction between COX-2 and p-Drp1^{Ser616} while the PLA focus was obviously increased (Fig. 2B). WB assays showed that the level of activated isoform of Drp1, p-Drp1^{Ser616}, was increased, while the levels of p-Drp1^{Ser637} and Mfn2 were decreased, by COX-2 overexpression (Fig. 2C). We also found the two

markers of cancer stemness, ABCG2 and Oct4 expression, were also upregulated by COX-2 overexpression (Fig. 2C). Consistently, higher SP ratios were observed in the two cell lines overexpressing COX-2 (Fig. 2D). In addition, the frequency of CSCs was 1/130.7 (95% CI, 1/141.3 to 1/121) and 1/82.8 (95% CI, 1/90.2 to 1/76) in CNE1-pBabe and CNE1-PTGS2 cell lines, while 1/127.1 (95% CI, 1/137.5 to 1/117) and 1/74.4 (95% CI, 1/81.4 to 1/68) in CNE2-pBabe and CNE2-PTGS2 cell lines. The frequency of CSCs increased about 1.57-fold and 1.70-fold in CNE1-PTGS2 and CNE2-PTGS2 cells, respectively, compared to the corresponding pBabe control cells (Fig. 2E). Based on these results, we deduced that COX-2 overexpression results in increase the activity of Drp1 and the upregulation of NPC stemness.

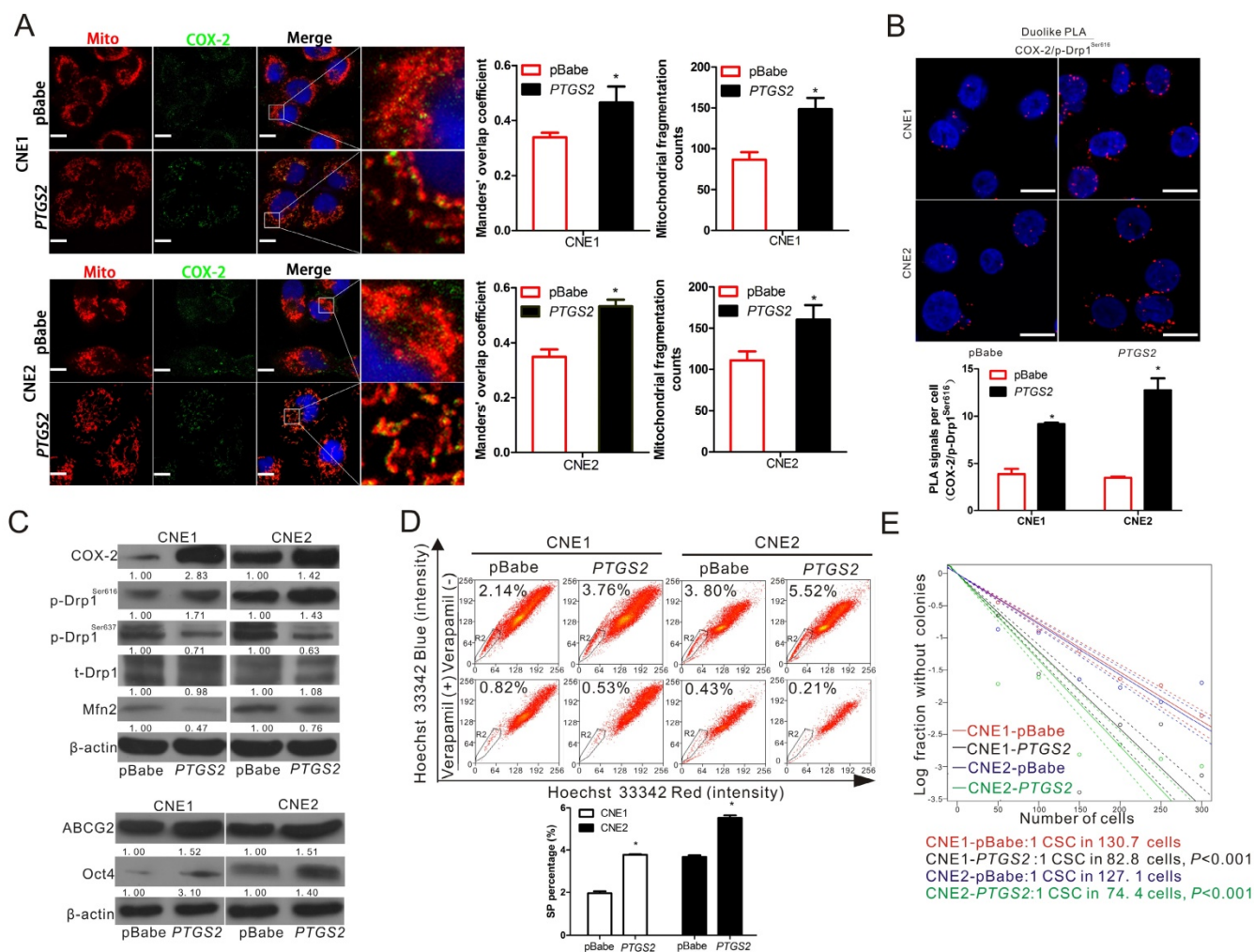


Figure 2. Upregulation of COX-2 leads to the activation of Drp1 and increases the cancer stemness of NPC. (A) Confocal microscopy images of CNE1-pBabe, CNE1-PTGS2, CNE2-pBabe, and CNE2-PTGS2 cell lines stained for COX-2 (green), mitochondria (red) and nuclei (blue). Manders' overlap coefficients for the co-localization of COX-2 with mitochondria and the mitochondrial fragmentation counts were calculated by IPP 6.0 and shown in right bar graphs. (B) The *in situ* proximity ligation assay (PLA) was used to detect interaction between COX-2 and p-Drp1^{Ser616} in CNE1-pBabe, CNE1-PTGS2, CNE2-pBabe, and CNE2-PTGS2 cells. Interaction events are shown as red dots (×630 magnification; scale bar, 20 μm). Quantification of COX-2/p-Drp1^{Ser616} interaction events are shown by bar charts (lower). (C) WBs showing the expression of COX-2, p-Drp1^{Ser616}, p-Drp1^{Ser637}, t-Drp1, Mfn2, ABCG2, and Oct4 in the CNE1 or CNE2 stable cell lines either overexpressing PTGS2 or transfected with control vector (pBabe). (D) The proportion of SP cells in the CNE1 or CNE2 stable cell lines overexpressing PTGS2 was analyzed by FCM. The R2 gate shows the SP cells. Representative examples are displayed. * P < 0.05 as compared with pBabe cells. (E) *In vitro* extreme limiting dilution assays to demonstrate the frequency of CSCs in CNE1-pBabe, CNE1-PTGS2, CNE2-pBabe, and CNE2-PTGS2 cell lines. The dashed lines show 95% confidence interval (CI) of the frequency of CSCs.

Inhibition of Drp1 or knockdown of DNMI1 downregulates cancer stemness of NPC

To further verify the relationship between COX-2 and Drp1 in mitochondria and the functional roles of these proteins in the regulation of cancer stemness, Mdivi-1, a selective molecule inhibitor which inhibiting the activation of Drp1 GTPase thereby decreasing the activity of Drp1 [30], was employed to treat CNE1 and CNE2 cells. We found that Mdivi-1 induced a significant decrease in the numbers of fragmented mitochondria (Fig. 3A), but did not affect the mitochondrial COX-2 (Fig. S4). Mdivi-1 was able to decrease p-Drp1^{Ser616} markedly

and increase the levels of p-Drp1^{Ser637} and Mfn2 without changing the expression of total Drp1 and COX-2 (Fig. 3B). In order to assess the inhibitory effect of Mdivi-1 on NPC stemness. WB, SP cell analysis, and colony formation assays were performed. These results showed that Mdivi-1 significantly downregulated the expression of ABCG2 and Oct4 (Fig. 3B) and decreased the percentages of SP cells (Fig. 3C) and colony formation (Fig. S5) in both CNE1 and CNE2 cells. To study the expression of Drp1 on the upregulation of stemness induced by COX-2 in NPC cells, we knocked down the expression of Drp1 by transfecting siDNMI1 into CNE1-PTGS2 and CNE2-PTGS2 cells. Compared with the negative

control (siNC), Drp1 knockdown decreased the mitochondrial fission induced by COX-2 overexpression, but did not affect the mitochondrial COX-2 in CNE1 and CNE2 cells (Fig. 4A, bar graphs; Fig. S6). WB assays showed that Drp1 knockdown caused a marked reduction of the expressions of ABCG2 and Oct4 (Fig. 4B, siDNM1L lanes), which were increased by upregulating COX-2 (Fig. 4B, PTGS2 lanes). The increased SP percentages caused by COX-2 overexpression decreased with the downregulation of Drp1 expression (Fig. 4C-D). Colony formation assays were consistent with FCM analysis (Fig. S7). To sum up, our findings suggest that the activity of Drp1 is regulated by COX-2 and

plays a crucial role in maintaining cancer stemness of NPC.

COX-2 knockdown decreases p-Drp1^{Ser616} and NPC stemness by lessening the mitochondrial translocation of p53

To further explore the underlying mechanism of the activation of Drp1 induced by COX-2, the stable COX-2-knockdown cell lines constructed in our previous study were used [9]. Immunofluorescence analysis showed that mitochondrial COX-2 was decreased and mitochondrial fragmentation counts were reduced in CNE1-shPTGS2 and CNE2-shPTGS2 cells (Fig. 5A, bar graphs).

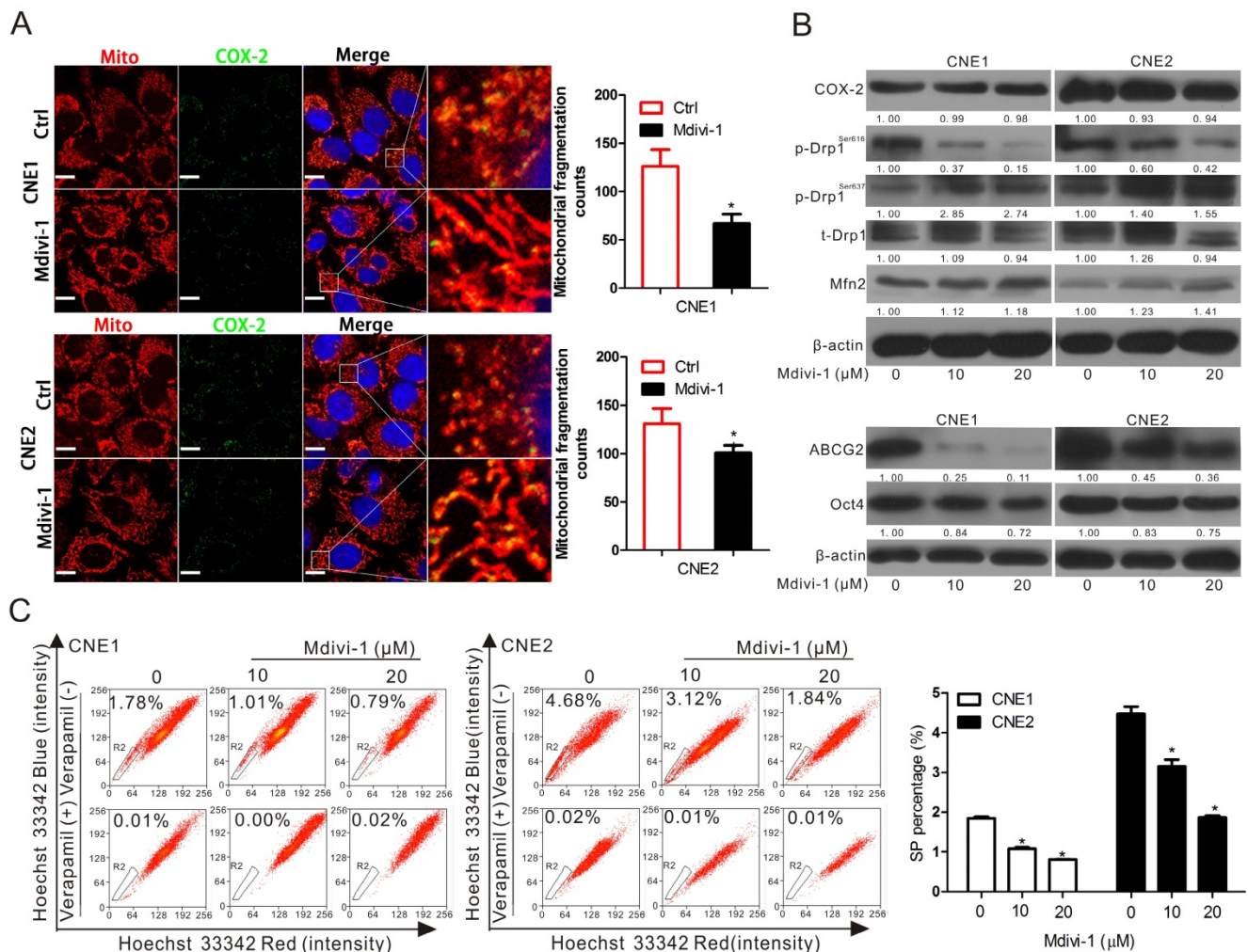


Figure 3. Inhibition of p-Drp1^{Ser616} by Mdivi-1 can downregulate cancer stemness but has no effect on COX-2. (A) CNE1 and CNE2 cells were treated with 20 μM Mdivi-1 for 24 h. The co-localization of COX-2 (green) and mitochondria (red) was examined by confocal microscopy, when nuclei are stained blue. Quantification of the mitochondrial fragmentation counts is shown in right bar graphs. Manders' overlap coefficients for the co-localization of COX-2 with mitochondria are shown in Fig.S4. (B) CNE1 and CNE2 cells were treated with or without various concentrations of Mdivi-1 (0, 10, or 20 μM) for 24 h and the level of COX-2, p-Drp1^{Ser616}, p-Drp1^{Ser637}, t-Drp1, Mfn2, ABCG2, and Oct4 in CNE1 and CNE2 cells were measured by WB assay. (C) SP cells were treated as in (B) and analyzed by FCM. Quantification are shown by bar graphs. * P < 0.05, compared with the Ctrl group.

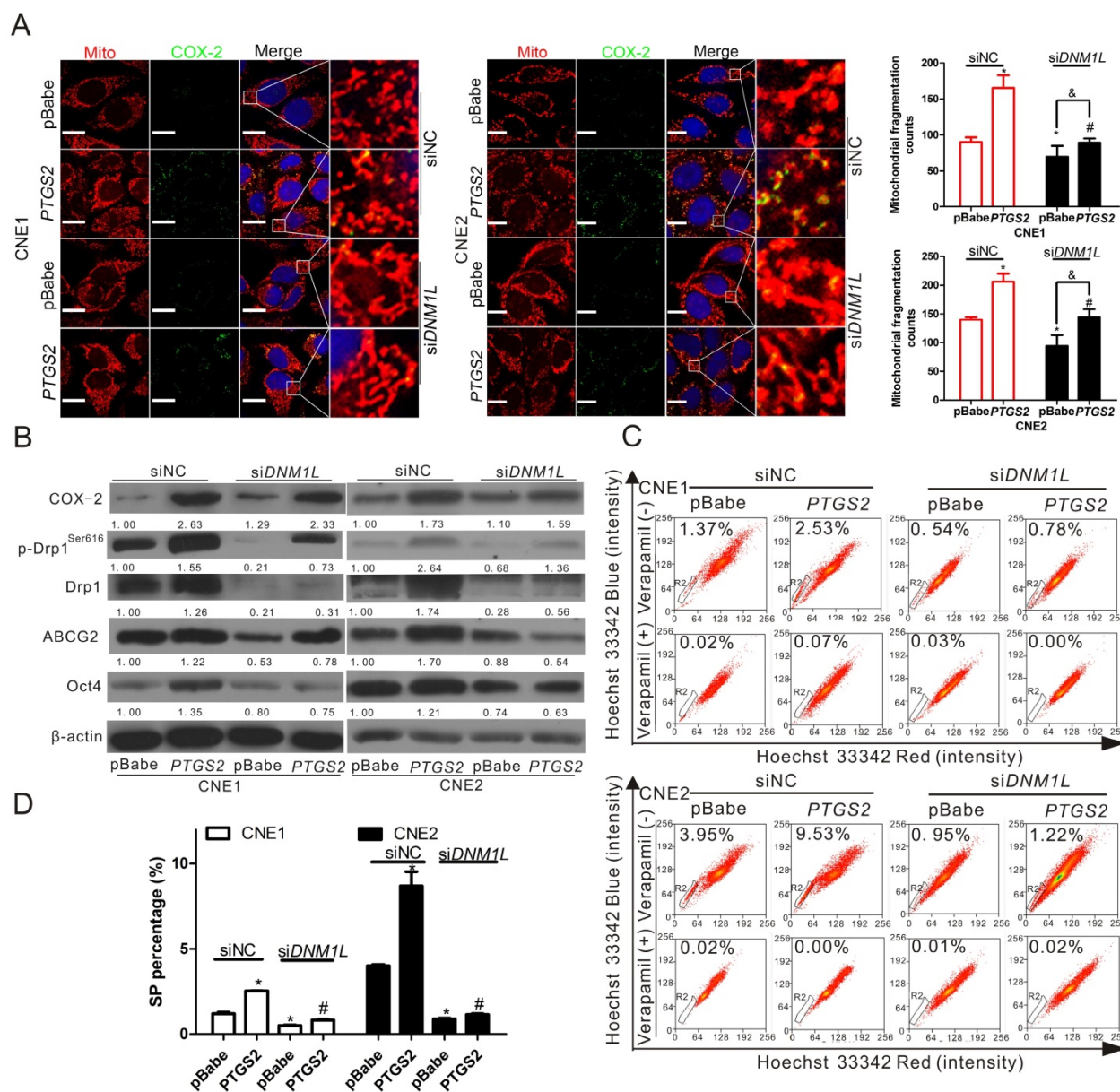


Figure 4. Knockdown of Drp1 by siDNM1L downregulates the increase of mitochondrial fission and NPC stemness induced by COX-2 overexpression. CNE1-pBabe, CNE1-PTGS2, CNE2-pBabe, and CNE2-PTGS2 cells were transfected with siNC or siDNM1L (50 nM) for 12 h. (A) The co-localization of COX-2 (green) and mitochondria (red) was determined by confocal microscopy. Quantification of the mitochondrial fragmentation counts is shown in bar graphs. (B) The expression level of COX-2, p-Drp1^{Ser616}, t-Drp1, ABCG2, and Oct4 was detected by WB assay. (C) SP cells were analyzed by FCM. (D) Quantification of SP cells in CNE1 and CNE2 are shown in bar graphs. * $P < 0.05$, compared with the CNE1-pBabe (siNC) or CNE2-pBabe (siNC) group. # $P < 0.05$, compared with the CNE1-PTGS2 (siNC) or CNE2-PTGS2 (siNC) group, & $P < 0.05$ compared with the CNE1-pBabe (siDNM1L) or CNE2-pBabe (siDNM1L) group.

PLA assays showed that COX-2 knockdown significantly reduced the interaction between COX-2 and p-Drp1^{Ser616} (Fig. 5B). Since p53-Drp1 complexes lead to mitochondrial fragmentation [31], we also measured the interaction between p53 and p-Drp1^{Ser616} and found it was significantly decreased by COX-2 knockdown (Fig. 5B). Moreover, by transfecting siPTGS2 or siNC into SP and MP cells sorted from CNE1 and CNE2 cells, we found that COX-2 and p-Drp1^{Ser616} interactions were higher in SP cells than in MP cells. Compared to siNC, COX-2 knockdown significantly reduced the interaction

between COX-2 and p-Drp1^{Ser616} in both SP and MP cells (Fig. 5C). We further measured the levels of COX-2, p53, and p-Drp1^{Ser616} in the whole cell lysates (WCL), mitochondrial fractions (Mito), and cytoplasmic fractions (Cyto) of CNE1-shPTGS2 and CNE2-shPTGS2 cells. These results showed that in WCL the level of p-Drp1^{Ser616} was decreased, while the levels of p-Drp1^{Ser637} and Mfn2 were increased after knockdown the expression of COX-2 (Fig. 5D). In subcellular fractions, mitochondrial p53 and p-Drp1^{Ser616} were inhibited by COX-2 knockdown and cytoplasmic p53 and p-Drp1^{Ser616} were increased (Fig.

5E). Also, the level of ABCG2 and Oct4 (Fig. 5F), and the percentage of SP (Fig. 5G-H), were all correspondingly downregulated. The frequencies of CSCs in CNE1-shCtrl and CNE1-shPTGS2 cells were 1/138.6 (95% CI, 1/149 to 1/128) and 1/233.4 (95% CI, 1/253 to 1/115), while in CNE2-shCtrl and CNE2-shPTGS2 cells the figures were 1/119.7 (95%

CI, 1/129 to 1/110) and 1/186.2 (95% CI, 1/202 to 1/172). COX-2 knockdown significantly decrease the frequency of CSCs compared to the corresponding shCtrl cells (Fig.5I). Taken together, these data indicated that p-Drp1^{Ser616} was regulated by the mitochondrial translocation of COX-2 and p53.

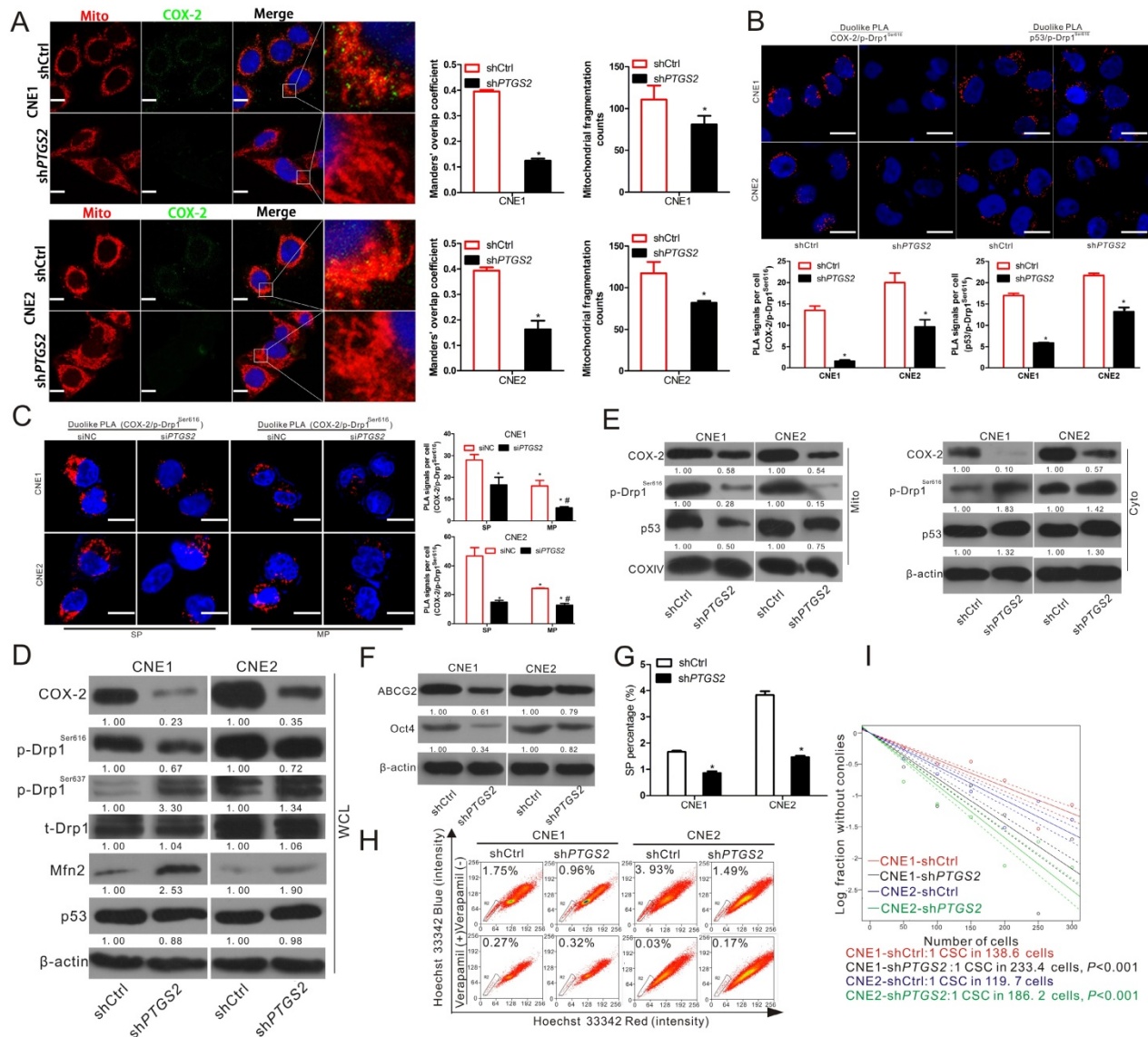


Figure 5. Inhibiting COX-2 expression decreases p-Drp1^{Ser616} and cancer stemness by lessening the mitochondrial translocation of p53. COX-2 knockdown cells, CNE1-shCtrl, CNE1-shPTGS2 CNE2-shCtrl, and CNE2-shPTGS2 cells were used. (A) The four cell lines stained for COX-2 (green), mitochondria (red) and nucleus (blue) were imaged by confocal microscopy. Manders' overlap coefficients for the co-localization of COX-2 with mitochondria and the mitochondrial fragmentation counts calculated by IPP 6.0 are shown in right bar graphs. (B) The *in situ* proximity ligation assay (PLA) shows the interactions of COX-2 with p-Drp1^{Ser616} and p53 with p-Drp1^{Ser616} in the four cell lines. Interaction events are shown as red dots (Scale bar: 20 μm). Quantification of p53/p-Drp1^{Ser616} and COX-2/p-Drp1^{Ser616} interaction events are shown in bar charts (lower). * *P* < 0.05 as compared with the shCtrl cells. (C) SP and MP cells were sorted from CNE1 and CNE2 cells and transfected with siNC or siPTGS2 (50 nM) for 12 h and the interaction between COX-2 and p-Drp1^{Ser616} was then detected with the PLA. Interaction events are shown as red dots (×630 magnification; scale bar, 20 μm). Quantifications of COX-2/p-Drp1^{Ser616} interaction events are shown by bar charts (right). * *P* < 0.05 as compared with CNE1-SP (siNC) or CNE2-SP (siNC), # *P* < 0.05 as compared with CNE1-MP (siNC) or CNE2-MP (siNC). (D-E) Whole cell lysates (WCL) and mitochondrial (Mito) and cytosolic (Cyto) fractions of in the four cell lines were subjected to WB assay. Expressions of COX-2, p-Drp1^{Ser616}, p-Drp1^{Ser637}, t-Drp1, and Mfn2 are shown for WCL, and COX-2, p53, and p-Drp1^{Ser616} are shown for the Mito and Cyto fractions. (F) Cell lysates of PTGS2-knockdown cell lines were subjected to WB for measurement of ABCG2 and Oct4. (G-H) SP cells in the four cell lines were analyzed by FCM and quantification is shown in the bar graphs. * *P* < 0.05 as compared with the shCtrl cells. (I) The frequencies of CSCs in PTGS2-knockdown cell lines were measured by *in vitro* extreme limiting dilution assays. The dashed lines show 95% confidence interval (CI) of the frequency of CSCs.

Resveratrol suppresses stemness in NPCs by inhibiting the mitochondrial COX-2

To confirm that the mitochondrial COX-2 is an effective therapeutic target for inhibiting stemness in NPC, CNE1 and CNE2 cells were treated with resveratrol (RSV), a natural phytochemical widely used for cancer chemoprevention. Non-steroidal anti-inflammatory drugs (NSAIDs), including celecoxib, aspirin and indomethacin, the selective inhibitors of COX-2, were also used for treatment. Either RSV or NSAIDs (aspirin and indomethacin) could downregulate the mitochondrial COX-2. Moreover, the co-localization of mitochondrial p53 and p-Drp1^{Ser616} were inhibited in CNE2 cells treated with NSAIDs (Fig. S8). We then chose RSV as a candidate drug to establish model for further study. As shown in Fig. 6A, RSV significantly suppressed mitochondrial COX-2, the mitochondrial translocation of p53, and mitochondrial fission in both CNE1 and CNE2 cells. Consistent with the data in Fig. 5, the p-Drp1^{Ser616} was decreased and p-Drp1^{Ser637} was correspondingly increased in the whole cellular extracts when the expression of COX-2 was downregulated by RSV (Fig. 6B). The expression levels of COX-2, p53, and p-Drp1^{Ser616} in the isolated mitochondria and cytoplasm were in perfect agreement with the immunofluorescence results (Fig. 6B). The levels of COX-2, ABCG2, and Oct4 (Fig. 6C), the SP fractions (Fig. 6D-E), and the areas of colony formation (Fig. S9) were decreased in a concentration-dependent manner in both CNE1 and CNE2 with RSV treatment. These results indicate that mitochondrial COX-2 is an effective target for decreasing NPC stemness. The inhibitional agents targeting to the mitochondrial COX-2 such as RSV might, therefore, be a potential therapeutic drug for sensitizing NPC to chemotherapy by inhibiting of stemness.

RSV sensitizes NPC cells to 5-FU through the inhibition of cancer stemness

Increasing numbers of studies indicate that inhibiting cancer stemness enhances the therapeutic efficacy of chemotherapy [32]. We therefore investigated whether RSV would sensitize NPC cells to 5-FU, a key drug in the treatment of NPC patients, since 5-FU, when administrated by itself, could increase the cancer stemness of NPC. Our results showed that the expressions of mitochondrial COX-2 and p53 as well as mitochondrial fission were increased in both CNE1 and CNE2 cells treated with 5-FU alone (Fig. 7A). These effects could be reversed by RSV (Fig. 7A). Upregulation of COX-2, p-Drp1^{Ser616}, ABCG2, and Oct4 induced by 5-FU were

also counteracted by RSV (Fig. 7B-C). Increases of SP ratio (Fig. 7C-D) and colony formation area (Fig. S10) caused by 5-FU were also decreased by RSV in CNE1 and CNE2 cells. Co-treatment of CNE1 and CNE2 cells with RSV and 5-FU resulted in cell viability decreases compared to cells in the 5-FU-only-treated group (Fig. 7E). In addition, we detected the cell apoptosis rate by FCM after treating CNE1 and CNE2 cells with Ctrl, 5-FU, RSV, or a combination of 5-FU and RSV. The results show that co-treatment with 5-FU and RSV induces a higher apoptosis rate (CNE1, 44.9%±0.62%, CNE2, 38.9%±1.04%) than treatment with either 5-FU (CNE1, 12.2%±0.77%, CNE2, 13.3%±0.87%) or RSV (CNE1, 19.1%±0.54%, CNE2, 20.5%±0.35%) alone (Fig. 7F). WB analysis was performed and found that co-treatment with 5-FU and RSV upregulates the expression levels of BAX, cleaved-caspase 3 (C-caspase 3), and LC3, and downregulates the expression level of Bcl-2 compared to 5-FU or RSV treatment alone (Fig. 7G). These data suggest that inhibition of the mitochondrial COX-2 with RSV sensitizes NPC cells to 5-FU via the suppression of cancer stemness.

Inhibition of COX-2 and p-Drp1^{Ser616} by RSV promotes the sensitivity of NPC xenograft tumors to 5-FU

To confirm that RSV sensitizes NPC to 5-FU *in vivo*, we examined the combination effect of RSV and 5-FU in an *in vivo* xenograft nude mice model using CNE2 cells (which have a higher percentage of SP cells than the CNE1 cell line). Our results showed that a combination of RSV with 5-FU led to a significant reduction in tumor volume (Fig. 8A-B) and weight (Fig. 8C) compared to untreated controls or animals treated with RSV or 5-FU alone. In order to see whether RSV sensitized NPC tumors to 5-FU via suppression of COX-2, p-Drp1^{Ser616}, and cancer stemness *in vivo*, WB and IHC analysis were employed. The results showed there was a significant reduction of COX-2, p-Drp1^{Ser616}, ABCG2, and Oct4 in the combination group compared with either control or 5-FU treatment alone (Fig. 8D-E). The *in vivo* study results are in perfect agreement with the *in vitro* study findings indicating that the mitochondrial COX-2 is a potential target for decreasing the stemness of NPC. Inhibition of the mitochondrial COX-2 by RSV increased the chemosensitivity of NPC tumors to 5-FU *in vivo*.

Discussion

The stemness of CSCs contributes to the resistance and relapse of NPC [26]. The identification of effective targets for decreasing NPC stemness is urgently required. Previous studies have

demonstrated that COX-2 plays an essential role in maintaining CSCs in such cancers as glioblastoma [33], osteosarcoma [34], and hepatocellular carcinoma [35]. Our previous study demonstrated that COX-2 is overexpressed in the CSCs of NPC and indicated it might be a novel therapeutic target for treating NPC [9]. In the present study, investigating the specific mechanism of the role of mitochondrial COX-2 in the

regulation of NPC stemness, the CSCs of NPC were enriched by flow cytometry. We found that NPC-CSCs possessed a significantly higher percentage of chippy mitochondria and a concomitant decrease of branched mitochondria compared with non-CSC of NPC, these results are consistent with research from Shen et al [14].

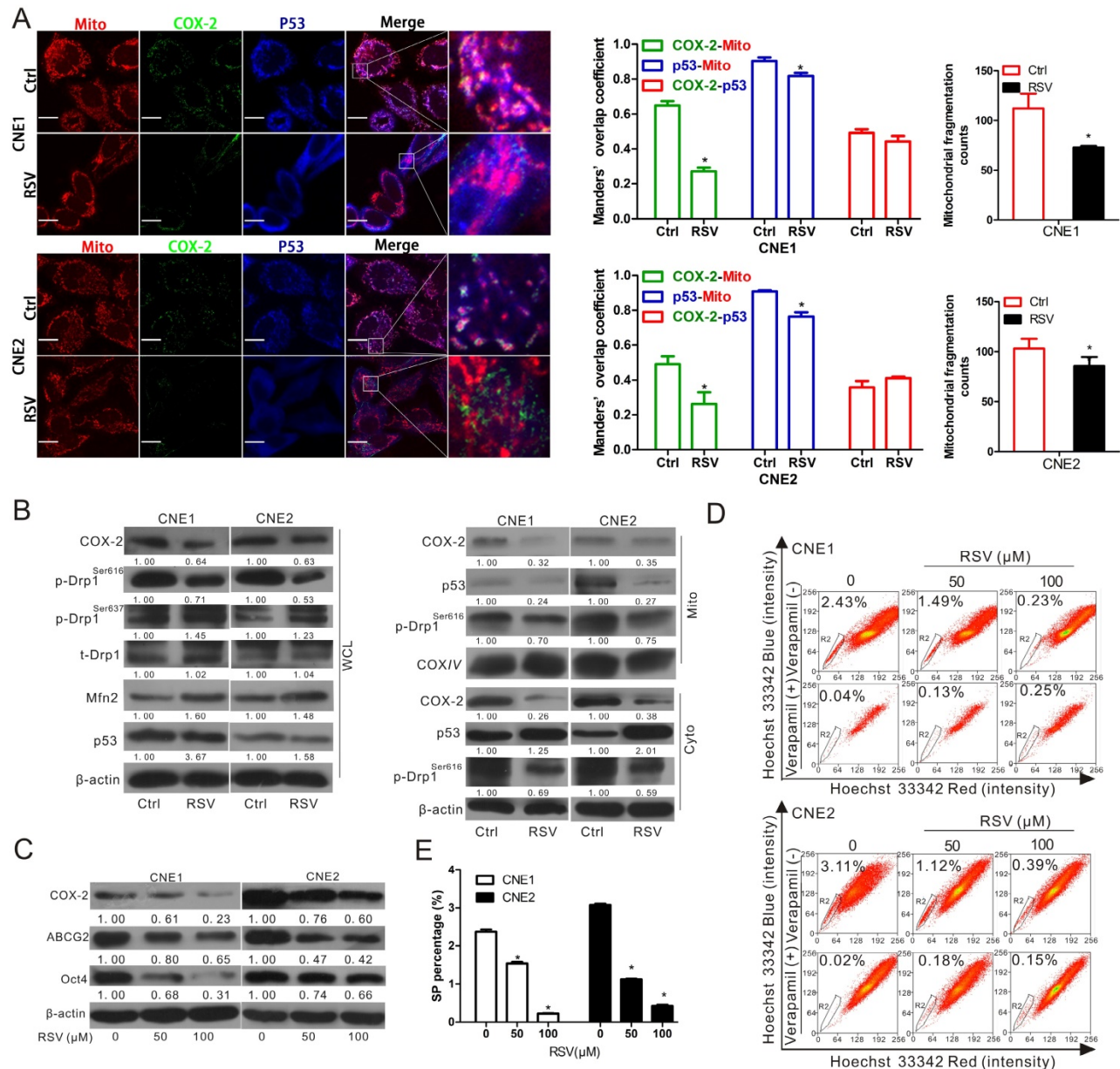


Figure 6. Resveratrol inhibits mitochondrial fission and induces the suppression of NPC stemness by reducing the mitochondrial localization of COX-2 and p53. (A-B) CNE1 and CNE2 cells were treated with or without 100 μM resveratrol (RSV) for 24 h. (A) Confocal microscopy images of CNE1 and CNE2 cells immunostained with anti-COX-2 (green), anti-p53 (blue) antibodies, and MitoTracker (red). Manders' overlap coefficients for the co-localization of COX-2-mitochondria, p53-mitochondria, and COX-2-p53 are shown. Mitochondrial fragmentation counts were calculated by IPP6.0 and shown in bar graphs. (B) Whole cell lysates (WCL) and mitochondrial (Mito) and cytosolic (Cyto) fractions of CNE1 and CNE2 cells with or without treatment were prepared. WB assays were performed to determine the expression levels of COX-2, p-Drp1^{Ser616}, p-Drp1^{Ser637}, t-Drp1 in WCL and those of COX-2, p53, p-Drp1^{Ser616} in Mito and Cyto fractions. (C-D) CNE1 and CNE2 cells treated with 0, 50, 100 μM RSV for 24 h were harvested. (C) COX-2, ABCG2 and Oct4 protein level was determined by WB assays. (D) The proportion of SP cells was analyzed by FCM. (E) Quantification of SP cells in CNE1 and CNE2 was shown in bar graphs. * P < 0.05, compared with the Ctrl group.

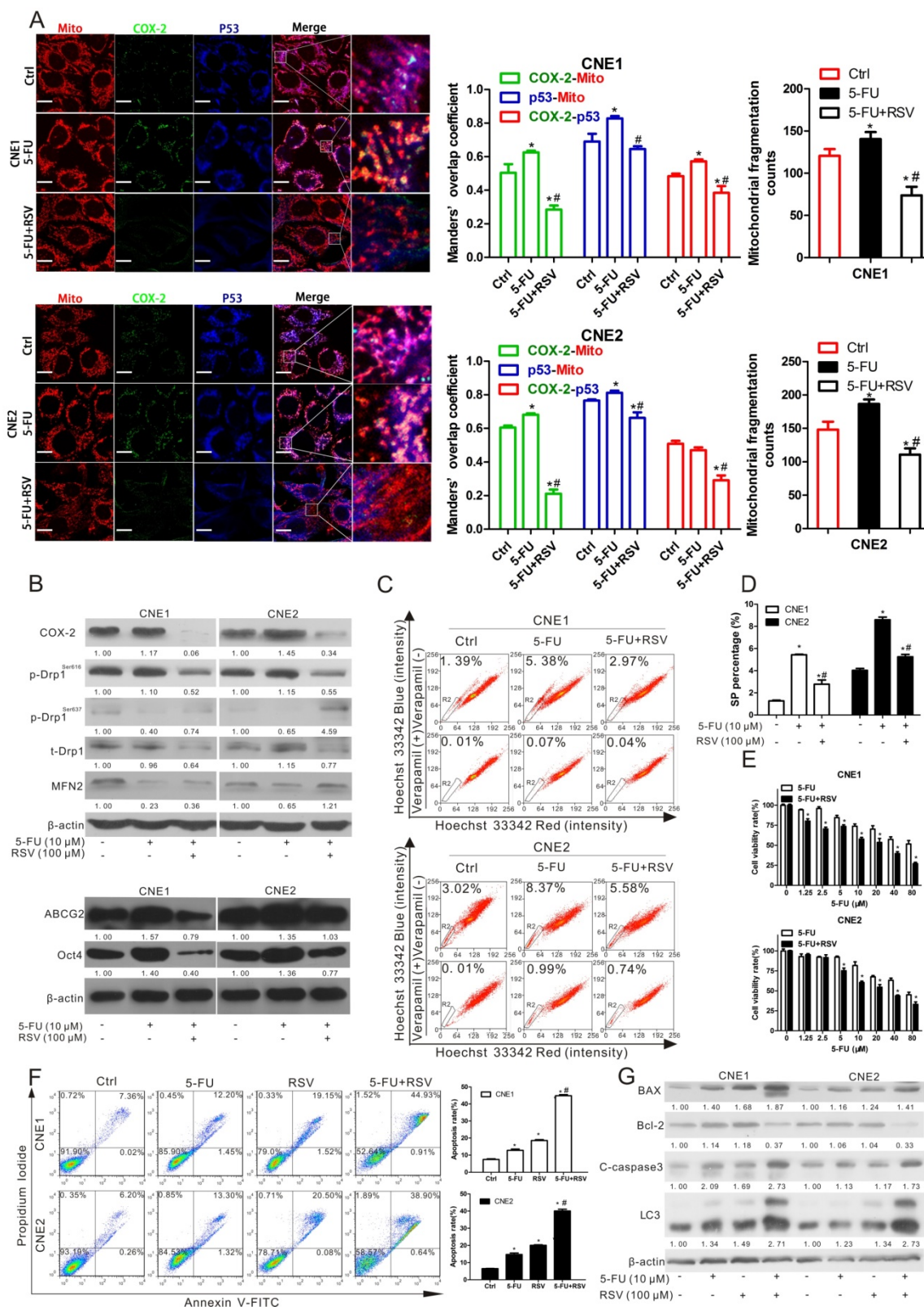


Figure 7. Resveratrol sensitizes NPC cells to 5-FU by decreasing COX-2 and p-Drp1^{Ser616}. (A-D) CNE1 and CNE2 cells were treated with 10 μM 5-FU in the presence or absence of resveratrol (RSV, 100 μM) for 24 h. (A) The co-localization of COX-2 (green), p53 (blue) and mitochondria (red) was imaged by confocal microscopy. Manders' overlap coefficients for the co-localization of COX-2 with mitochondria and the mitochondrial fragmentation counts were shown in bar graphs. (B) Expression of COX-2, p-Drp1^{Ser616}, p-Drp1^{Ser637}, t-Drp1, Mfn2, ABCG2 and Oct4 were detected using WB assay. (C) SP cells were measured by FCM. (D) Quantification of SP cells in CNE1 and CNE2 was shown in bar graphs. * $P < 0.05$, compared with the Ctrl group. # $P < 0.05$, compared with the 5-FU alone group. (E) CNE1 and CNE2 cells were treated with increasing concentrations of 5-FU (1.25–80 μM) with or without RSV (100 μM) for 24 h, and cell viability was measured with the MTT assay. * $P < 0.05$ for combination treatment vs. 5-FU alone. (F-G) CNE1 and CNE2 cells were treated with Ctrl, 5-FU (10 μM), RSV (100 μM) or a combination of 5-FU and RSV for 24 h. (F) The cell apoptosis rate detected by Annexin V-FITC assay and analyzed by FCM. * $P < 0.05$ as compared with Ctrl group, # $P < 0.05$ as compared with 5-FU alone group. (G) Expressions of BAX, Bcl-2, cleaved-caspase 3, and LC3 as detected using WB assay.

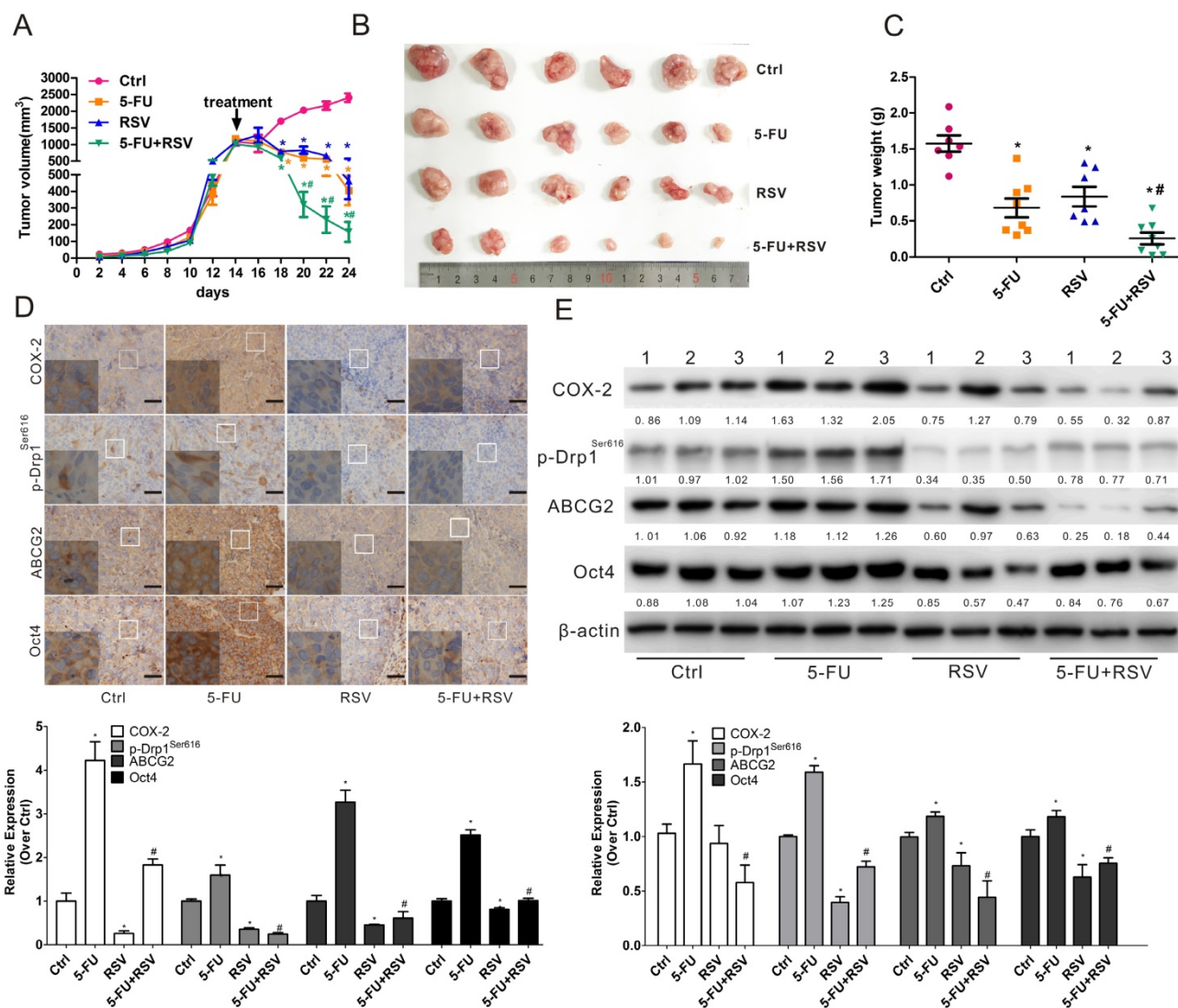


Figure 8. Resveratrol enhances the sensitivity of NPC to 5-FU in vivo. Nude mice bearing CNE2 cells as primary xenografts were randomly separated into 4 groups (n=6) and injected by tail vein with physiological saline (Ctrl), 5-FU (2 mg/kg), resveratrol (RSV, 50 mg/kg) or a combination of 5-FU and RSV every other days for five times. (A) The growth curves of the tumors in the four groups. Tumor volume=1/2 × length × width². (B) Representative images of the xenograft tumors in the four groups. (C) Tumor weights in the four groups. (D) Sections of tumors were subjected IHC for evaluating the expression of COX-2, p-Drp1^{Ser616}, ABCG2, and Oct4. Scale bars, 50 μm. The relative amounts of COX-2, p-Drp1^{Ser616}, ABCG2 and Oct4 proteins determined by IPP 6.0 analysis are shown in the bar graphs (lower). (E) WB assays were employed to measure the expression levels of COX-2, p-Drp1^{Ser616}, ABCG2, and Oct4 in representative tumor tissues (n=3). Quantification of the expression levels are shown in the bar graphs (lower photograph). * P < 0.05 for RSV, or 5-FU alone vs. control. # P < 0.05 for combination treatment vs. 5-FU alone.

Other studies have clarified the critical role of COX-2/PGE2 and Drp1 in tumor carcinogenesis and therapeutics. Using transgenic mice, Pan et al showed that COX-2/PGE2 promotes lung tumor development via the MAPK pathway, cell proliferation and transformation were inhibited in K-ras/COX-2^{-/-} mice [36]. Another study from Cao et al, using K19-C2mE transgenic mice, revealed that COX-2/PGE2 signal transduction was involved in the initiation and progression of gastric tumors [37]. Moreover, overexpression COX-2 was correlated with poor prognosis for breast carcinoma patients [38]. Drp1-dependent mitochondrial division also was

essential for MAPK-driven malignancies [39]. Serasinghe et al found that p-Drp1^{S616} plays a mechanistic role in oncogenic RASG12V-mediated cellular transformation [40]. The nuclear expression of Drp1 has a similar effect in lung adenocarcinomas [23], and correlates with patients' tumor recurrence and poor prognosis [41]. Either deletion of COX-2/PGE2 or inhibition of Drp1 could enhance the sensitivity to chemotherapy of various tumors. However the relation between mitochondrial COX-2/Drp1 and the progression of NPC has rarely been reported. In the current study, we have demonstrated that both COX-2 and Drp1 are

upregulated in the tumors of NPC patients and in the stem-like SP cells of NPC cell lines. Based on both the above mentioned researches and our data, we have reached the conclusion that mitochondrial co-localization of COX-2 and Drp1 has significance for the theranostics of NPC.

Drp1 is an important mediator of mitochondrial fission. Our data showed that p-Drp1^{Ser616}, the activated form of Drp1, was significantly increased in NPC-CSCs. Moreover, we found that Drp1 was upregulated in radio-resistant NPC tumors tissues from the GEO database. We thus deduced that both COX-2 and Drp1 are closely linked to NPC cancer stemness. Interestingly, COX-2 and Drp1 showed a strong positive correlation in the samples of NPC patients. These data indicated that the promotion of mitochondrial fission and the excessive activity of Drp1 is the possible mechanism for increasing cancer stemness by COX-2.

Many studies have confirmed that p-Drp1^{Ser616} is a promising therapeutic target for cancer [17, 42-44]. Exploring the mechanism of Drp1 activation is therefore significant for understanding its clinical application. Many functional kinases or protein phosphatases are involved in the regulation of Drp1 activity. Wang et al. reported that the mitochondrial protein phosphatase PGAM5 decreasing the activity of Drp1 by dephosphorylating p-Drp1^{Ser637} [45]. Cyclin-dependent kinase 1 (CDK1) and CDK5 regulate Drp1 Ser616 phosphorylation and increase its activity [17]. Herein, using stable *PTGS2*-knockdown and -overexpression cell lines, we for the first time found that mitochondrial COX-2 increase the activation of Drp1 by recruiting the mitochondrial translocation of p53. Moreover, inhibition of the GTPase activity of Drp1 with Mdivi-1 had no effect on the expression of mitochondrial COX-2 but significantly downregulated the stemness of NPC. Knockdown the expression of Drp1 by *siDNM1L* further showed that mitochondrial COX-2 is an upstream regulator of the function of Drp1 in mitochondrial fission. Another recent study provided the other mechanistic insight into their relationship by showing that mitochondrial fission could regulate mitochondrial ROS production and induce the expression of COX-2 through the activation of NF- κ B [46]. Further work is needed to identify the regulatory relationship between COX-2 and Drp1.

It is known that Drp1, a downstream mediator of p53, can increase the activity of Drp1 by its mitochondrial translocation [47, 48]. Many studies have demonstrated that COX-2 and p53 may form a complex and regulate the expression of p53-responsive genes [49, 50]. In this study, we found that COX-2 knockdown in NPC decreases the

co-localization of mitochondrial COX-2 and p53, reducing mitochondrial fission and decreasing cancer stemness. Yet other results have demonstrated that abundant mitochondrial translocation of COX-2 in cancer cells confers resistance to apoptosis [10]. In sum, we conclude that (1) mitochondrial COX-2 activates Drp1 by interacting with p53 and (2) mitochondrial COX-2 could be a theranostic target for reducing NPC cancer stemness. Our study confirmed that RSV suppresses the activity of Drp1 mainly by the regulation of mitochondrial COX-2 and p53. The suppression of mitochondrial COX-2 is the main contributor to the decrease of cancer stemness. The data confirmed that mitochondrial COX-2 is an effective target and targeting inhibition to its co-localization might increase the chemotherapy sensitivity of NPC.

Studies have reported that Drp1-dependent mitochondrial fission and fragmentation contribute to maintenance of stemness [51]. In brain tumor-initiating cells (BTICs), p-Drp1^{Ser616}-controlled mitochondrial fission serves a critical role in the process of stemness maintenance through downregulation of AMPK α activation [17]. In NPC, mitochondrial fission and its peri-nuclear distribution induced a switch from oxidative phosphorylation to glycolysis, which was considered the underlying mechanism of acquisition of stemness properties [14]. Javier et al have found that Drp1-dependent mitochondrial fission controlled by Erk was an early and necessary process for the generation of iPS (induced pluripotent stem) cells [52]. COX-2 in the tumor microenvironment was critical for the induction and maintenance of cancer stemness [53]. It is known a hypoxic microenvironment and hypoxia-inducible factor-1 α (HIF-1 α) perform a critical role in maintaining the stemness of CSCs [54, 55]. Csiki et al reported that HIF-1 α activated the transcription of COX-2 by interaction with the *PTGS2* promoter in non-small cell lung cancer cell [56]. Here, treating with the hypoxic mimetic agent cobalt chloride (CoCl₂) in CNE2 cells or SP and MP cells sorted from CNE2 cells, we found the tumor hypoxic microenvironment in NPC cells could promote mitochondrial fission in NPC-CSCs and increase the cancer stemness via upregulate mitochondrial COX-2 (data not shown). Our current study has provided proof for the idea that mitochondrial COX-2 in the tumor microenvironment induces generation of CSC through increased Drp1-dependent mitochondrial fission.

Both COX-2 and Drp1 play vital roles in the resistance to various chemotherapy drugs by promoting cancer cells' anti-apoptosis [57], migration, invasion [44], and cell cycle progression [23, 58]. It has

been reported that liensinine increases the susceptibility of breast cancer cells to a variety of chemotherapy drugs by inhibiting Drp1 mediated mitochondrial fission and mitophagy [59]. 5-FU is widely used in NPC treatment, but its chemo-resistance remains a significant limitation to its clinical application [60]. One of the mechanisms of resistance to 5-FU found in the present study is that it induces the overexpression of COX-2, the activation of Drp1, and the enrichment of CSCs in NPC. We also examined the combined effects of RSV, as an inhibitor of mitochondrial COX-2/p-Drp1 pathway, and 5-FU. *In vitro*, RSV suppresses the stemness of NPC evoked by 5-FU. *In vivo*, RSV sensitizes NPC tumors to 5-FU by significantly increase its inhibitory effect of NPC tumor growth. The molecular mechanism which RSV sensitizes NPC tumor to 5-FU is that RSV reduces mitochondrial COX-2 and p53 and inhibits mitochondrial fission and cancer stemness. This combination of RSV with 5-FU-based chemotherapy would represent an effective therapeutic strategy for NPC tumors.

It was reported that the use of drugs targeted to COX-2 and Drp1 was of great value for tumor prevention and treatment [42, 61]. Nonsteroidal anti-inflammatory drugs (NSAIDs) and various COX-2 selective inhibitors have been used in clinical treatment of various tumors, including colon, breast, lung, ovary, prostate, and urinary bladder cancer [62, 63]. Our results also showed that three different NSAIDs (aspirin, celecoxib, and indomethacin) and a selective COX-2 inhibitor, resveratrol, exert anti-tumor activity, primarily by the inhibition of mitochondrial COX-2 in NPC cells. Recent research has found that metformin, the first-line drug for the treatment of type 2 diabetes, can markedly lower the level of Drp1 and suppress atherosclerosis in diabetic mice in an AMPK-dependent manner [64]. Interestingly, it was shown that metformin has anti-tumor potential and its use in cancer prevention and treatment may suppress Drp1-mediated mitochondrial fission [65, 66]. Other studies have found that several small molecules, including Mdivi-1 [67], P110 [31], and melatonin [68], suppress on Drp1-dependent mitochondria fission. It was reported that resveratrol suppress COX-2 and Drp1-dependent mitochondrial fission [65, 69, 70], and resveratrol is continuing to be studied for cancer chemoprevention and treatment [71]. Our present study offers a proof that resveratrol functionalized its anti-tumor activity by inhibiting mitochondrial COX-2 and Drp1. Exploring the effects of these various inhibitors on tumors should be helpful for the application in clinical trials and for developing new anti-tumor drugs.

In summary, our current work provides new insights regarding the mechanisms of enhancing the activation of Drp1 by mitochondrial translocation of COX-2 and p53. We also demonstrate that inhibition of mitochondrial COX-2 can suppress the cancer stemness of NPC and mitochondrial COX-2 is a promising theranostic target for NPC treatment.

Supplementary Material

Supplementary figures and tables.

<http://www.thno.org/v07p1389s1.pdf>

Abbreviations

ABCG2: ATP-binding cassette sub-family G member 2
 ALDH1: aldehyde dehydrogenase 1
 BAX: Bcl-2-associated X protein
 Bcl-2: B-cell lymphoma protein 2
 BMI1: B lymphoma Mo-MLV insertion region 1 homolog
 COX-2: cyclooxygenase-2
 CSCs: cancer stem cells
 DAPI: 4, 6-diamidino-2-phenylindole
 Drp1: dynamin-related protein 1
 DNMI1: Dynamin 1-like gene (for Drp1)
 FCM: flow cytometry
 GEO: gene expression omnibus database at NCBI (NIH)
 HIF-1 α : hypoxia-inducible factor-1 α
 IHC: immunohistochemistry
 MFC: mitochondrial fragmentation counts
 MP: main population of cells
 MTT: 3-(4, 5-dimethylthiazol-2-yl)-2, 5-diphenyltetrazolium bromide
 NPC: nasopharyngeal carcinoma
 Oct4: octamer-binding transcription factor 4
 OD: optical density
 PTGS2: prostaglandin-endoperoxide synthase 2 gene (for COX-2)
 SP: side population of cells
 RSV: resveratrol
 WB: Western blotting
 5-FU: 5-fluorouracil

Acknowledgements

We thank Drs. William Melchior and Lei Guo for English editing. This work was supported by grants from the National Natural Science Foundation of China (NSFC Nos. 81472997, 81573181, 81402648), the Natural Science Foundation of Fujian Province of China (No. 2014J01372, 2015J01344), Xiamen Municipal Bureau of Ocean and Fisheries (14PYY051SF04), Early-stage Project of National Key Basic Research Program of China (No. 2014CB560710), Key Program (No. 81130052) of NSFC.

Competing Interests

The authors have declared that no competing interest exists.

References

- Yu MC, Yuan JM. Epidemiology of nasopharyngeal carcinoma. *Semin Cancer Biol.* 2002; 12:421-9.
- Wang WJ, Wu SP, Liu JB, Shi YS, Huang X, Zhang QB, et al. MYC regulation of CHK1 and CHK2 promotes radioresistance in a stem cell-like population of nasopharyngeal carcinoma cells. *Cancer Res.* 2013; 73:1219-31.
- Lee AW, Poon Y, Foo W, Law SC, Cheung FK, Chan DK, et al. Retrospective analysis of 5037 patients with nasopharyngeal carcinoma treated during 1976-1985: overall survival and patterns of failure. *Int J Radiat Oncol.* 1992; 23:261-70.
- Yang CF, Peng LX, Huang TJ, Yang GD, Chu QQ, Liang YY, et al. Cancer stem-like cell characteristics induced by EB virus-encoded LMP1 contribute to radioresistance in nasopharyngeal carcinoma by suppressing the p53-mediated apoptosis pathway. *Cancer Lett.* 2014; 344:260-71.
- Qin J, Ji J, Deng R, Tang J, Yang F, Feng GK, et al. DC120, a novel AKT inhibitor, preferentially suppresses nasopharyngeal carcinoma cancer stem-like cells by downregulating Sox2. *Oncotarget.* 2015; 6:6944-58.
- Wei P, Niu M, Pan S, Zhou Y, Shuai C, Wang J, et al. Cancer stem-like cell: a novel target for nasopharyngeal carcinoma therapy. *Stem Cell Res Ther.* 2014; 5:44.
- Rizzo MT. Cyclooxygenase-2 in oncogenesis. *Clin Chim Acta.* 2011; 412:671-87.
- Shi D, Xiao X, Tian Y, Qin L, Xie F, Sun R, et al. Activating enhancer-binding protein-2alpha induces cyclooxygenase-2 expression and promotes nasopharyngeal carcinoma growth. *Oncotarget.* 2015; 6:5005-21.
- Liao K, Xia B, Zhuang QY, Hou MJ, Zhang YJ, Luo B, et al. Parthenolide inhibits cancer stem-like side population of nasopharyngeal carcinoma cells via suppression of the NF-kappaB/COX-2 pathway. *Theranostics.* 2015; 5:302-21.
- Liou JY, Aleksic N, Chen SF, Han TJ, Shyue SK, Wu KK. Mitochondrial localization of cyclooxygenase-2 and calcium-independent phospholipase A 2 in human cancer cells: implication in apoptosis resistance. *Exp Cell Res.* 2005; 306:75-84.
- Wen SJ, Zhu DQ, Huang P. Targeting cancer cell mitochondria as a therapeutic approach. *Future Med Chem.* 2013; 5:53-67.
- Lamb R, Harrison H, Hulit J, Smith DL, Lisanti MP, Sotgia F. Mitochondria as new therapeutic targets for eradicating cancer stem cells: Quantitative proteomics and functional validation via MCT1/2 inhibition. *Oncotarget.* 2014; 5:11029-37.
- Alvero AB, Montagna MK, Holmberg JC, Craveiro V, Brown D, Mor G. Targeting the mitochondria activates two independent cell death pathways in ovarian cancer stem cells. *Mol Cancer Ther.* 2011; 10:1385-93.
- Shen YA, Wang CY, Hsieh YT, Chen YJ, Wei YH. Metabolic reprogramming orchestrates cancer stem cell properties in nasopharyngeal carcinoma. *Cell Cycle.* 2015; 14:86-98.
- Westermann B. Mitochondrial fusion and fission in cell life and death. *Nat Rev Mol Cell Biol.* 2010; 11:872-84.
- Todd LR, Gomathinayagam R, Sankar U. A novel Gfer-Drp1 link in preserving mitochondrial dynamics and function in pluripotent stem cells. *Autophagy.* 2010; 6:821-2.
- Xie Q, Wu Q, Horbinski CM, Flavahan WA, Yang K, Zhou W, et al. Mitochondrial control by DRP1 in brain tumor initiating cells. *Nat Neurosci.* 2015; 18:501-10.
- Otera H, Mihara K. Molecular mechanisms and physiologic functions of mitochondrial dynamics. *J Biochem.* 2011; 149:241-51.
- Kasahara A, Cipolat S, Chen Y, Dorn GW, Scorrano L. Mitochondrial fusion directs cardiomyocyte differentiation via calcineurin and Notch signaling. *Science.* 2013; 342:734-7.
- Vazquez-Martin A, Cufi S, Corominas-Faja B, Oliveras-Ferreros C, Vellon L, Menendez JA. Mitochondrial fusion by pharmacological manipulation impedes somatic cell reprogramming to pluripotency: new insight into the role of mitophagy in cell stemness. *Aging (Albany NY).* 2012; 4:393-401.
- Jang M, Cai L, Udeani GO, Slowing KV, Thomas CF, Beecher CW, et al. Cancer chemopreventive activity of resveratrol, a natural product derived from grapes. *Science.* 1997; 275:218-20.
- Hu Y, Smyth GK. ELDA: extreme limiting dilution analysis for comparing depleted and enriched populations in stem cell and other assays. *J Immunol Methods.* 2009; 347:70-8.
- Rehman J, Zhang HJ, Toth PT, Zhang Y, Marsboom G, Hong Z, et al. Inhibition of mitochondrial fission prevents cell cycle progression in lung cancer. *FASEB J.* 2012; 26:2175-86.
- Zhuang Q, Zhou T, He C, Zhang S, Qiu Y, Luo B, et al. Protein phosphatase 2A-B55b enhances chemotherapy sensitivity of human hepatocellular carcinoma under the regulation of microRNA-133b. *J Exp Clin Cancer Res.* 2016; 35:67.
- Zinchuk V, Grossenbacher-Zinchuk O. Recent advances in quantitative colocalization analysis: focus on neuroscience. *Prog Histochem Cytochem.* 2009; 44:125-72.
- Wang J, Guo LP, Chen LZ, Zeng YX, Lu SH. Identification of cancer stem cell-like side population cells in human nasopharyngeal carcinoma cell line. *Cancer Res.* 2007; 67:3716-24.
- Zhou S, Schuetz JD, Bunting KD, Colapietro AM, Sampath J, Morris JJ, et al. The ABC transporter Bcrp1/ABCG2 is expressed in a wide variety of stem cells and is a molecular determinant of the side-population phenotype. *Nat Med.* 2001; 7:1028-34.
- Koo B, Lee S, Kim J, Huang S, Kim S, Rho Y, et al. Oct4 is a critical regulator of stemness in head and neck squamous carcinoma cells. *Oncogene.* 2015; 34:2317-24.
- Chen H, Detmer SA, Ewald AJ, Griffin EE, Fraser SE, Chan DC. Mitofusins Mfn1 and Mfn2 coordinately regulate mitochondrial fusion and are essential for embryonic development. *J Cell Biol.* 2003; 160:189-200.
- Tanaka A, Youle RJ. A chemical inhibitor of DRP1 uncouples mitochondrial fission and apoptosis. *Mol Cell.* 2008; 29:409-10.
- Guo X, Disatnik M-H, Monbureau M, Shamloo M, Mochly-Rosen D, Qi X. Inhibition of mitochondrial fragmentation diminishes Huntington's disease-associated neurodegeneration. *J Clin Invest.* 2013; 123:5371-88.
- Monteiro J and Fodde R. Cancer stemness and metastasis: therapeutic consequences and perspectives. *Eur J Cancer.* 2010; 46:1198-203.
- Annabi B, Laflamme C, Sina A, Lachambre MP, Béliveau R. A MT1-MMP/NF-kappaB signaling axis as a checkpoint controller of COX-2 expression in CD133+ U87 glioblastoma cells. *J Neuroinflammation.* 2009; 6:8.
- Pang LY, Gatenby EL, Kamida A, Whitelaw BA, Hupp TR, Argyle DJ. Global gene expression analysis of canine osteosarcoma stem cells reveals a novel role for COX-2 in tumour initiation. *PLoS One.* 2014; 9:e83144.
- Guo Z, Jiang JH, Zhang J, Yang HJ, Yang FQ, Qi YP, et al. COX-2 promotes migration and invasion by the side population of cancer stem cell-like hepatocellular carcinoma cells. *Medicine (Baltimore).* 2015; 94:e1806.
- Pan Y, Jiang Y, Tan L, Ravoori MK, Gagea M, Kundra V, et al. Deletion of cyclooxygenase-2 inhibits K-ras-induced lung carcinogenesis. *Oncotarget.* 2015; 6:38816-26.
- Cao D, Jiang J, Tsukamoto T, Liu R, Ma L, Jia Z, et al. Canolol inhibits gastric tumors initiation and progression through COX-2/PGE2 pathway in K19-C2mE transgenic mice. *PLoS One.* 2015; 10:e0120938.
- Misron NA, Looi LM and Nik Mustapha NR. Cyclooxygenase-2 expression in invasive breast carcinomas of no special type and correlation with pathological profiles suggest a role in tumorigenesis rather than cancer progression. *Asian Pac J Cancer Prev.* 2015; 16:1553-8.
- Kashatus JA, Nascimento A, Myers LJ, Sher A, Byrne FL, Hoehn KL, et al. Erk2 phosphorylation of Drp1 promotes mitochondrial fission and MAPK-driven tumor growth. *Mol Cell.* 2015; 57:537-51.
- Serasinghe MN, Wieder SY, Renault TT, Elkholi R, Ascioia JJ, Yao JL, et al. Mitochondrial division is requisite to RAS-induced transformation and targeted by oncogenic MAPK pathway inhibitors. *Mol Cell.* 2015; 57:521-36.
- Chiang YY, Chen SL, Hsiao YT, Huang CH, Lin TY, Chiang IP, et al. Nuclear expression of dynamin-related protein 1 in lung adenocarcinomas. *Mod Pathol.* 2009; 22:1139-50.
- Qian W, Wang J and Van Houten B. The role of dynamin-related protein 1 in cancer growth: a promising therapeutic target? *Expert Opin Ther Targets.* 2013; 17:997-1001.
- Wang JN, Hansen K, Edwards R, Van Houten B and Qian W. Mitochondrial division inhibitor 1 (mdivi-1) enhances death receptor-mediated apoptosis in human ovarian cancer cells. *Biochem Biophys Res Commun.* 2015; 456:7-12.
- Zhao J, Zhang J, Yu M, Xie Y, Huang Y, Wolff DW, et al. Mitochondrial dynamics regulates migration and invasion of breast cancer cells. *Oncogene.* 2013; 32:4814-24.
- Wang Z, Jiang H, Chen S, Du F and Wang X. The mitochondrial phosphatase PGAM5 functions at the convergence point of multiple necrotic death pathways. *Cell.* 2012; 148:228-43.
- Park J, Choi H, Min JS, Park SJ, Kim JH, Park HJ, et al. Mitochondrial dynamics modulate the expression of pro-inflammatory mediators in microglial cells. *J Neurochem.* 2013; 127:221-32.
- Dashzeveg N and Yoshida K. Cell death decision by p53 via control of the mitochondrial membrane. *Cancer Lett.* 2015; 367:108-12.
- Guo X, Sesaki H and Qi X. Drp1 stabilizes p53 on the mitochondria to trigger necrosis under oxidative stress conditions in vitro and in vivo. *Biochem J.* 2014; 461:137-46.
- Chin Y-T, Yang S-H, Chang T-C, Changou CA, Lai H-Y, Fu E, et al. Mechanisms of dihydrotestosterone action on resveratrol-induced anti-proliferation in breast cancer cells with different ERα status. *Cancer.* 2015; 22:25-7.
- Corcoran CA, He Q, Huang Y and Sheikh MS. Cyclooxygenase-2 interacts with p53 and interferes with p53-dependent transcription and apoptosis. *Oncogene.* 2005; 24:1634-40.
- Senft D and Ronai ZA. Regulators of mitochondrial dynamics in cancer. *Curr Opin Cell Biol.* 2016; 39:43-52.
- Prieto J, Leon M, Ponsoda X, Sendra R, Bort R, Ferrer-Lorente R, et al. Early ERK1/2 activation promotes DRP1-dependent mitochondrial fission necessary for cell reprogramming. *Nat Commun.* 2016; 7:11124.
- Chimal-Ramirez GK, Espinoza-Sanchez NA and Fuentes-Panana EM. A role for the inflammatory mediators cox-2 and metalloproteinases in cancer stemness. *Anticancer Agents Med Chem.* 2015; 15:837-55.
- Carnero A and Leonart M. The hypoxic microenvironment: A determinant of cancer stem cell evolution. *Bioessays.* 2016; 38 (Suppl 1):S65-S74.

55. Marie-Egyptienne DT, Lohse I and Hill RP. Cancer stem cells, the epithelial to mesenchymal transition (EMT) and radioresistance: potential role of hypoxia. *Cancer Lett.* 2013; 341:63-72.
56. Csiki I, Yanagisawa K, Haruki N, Nadaf S, Morrow JD, Johnson DH, et al. Thioredoxin-1 modulates transcription of cyclooxygenase-2 via hypoxia-inducible factor-1alpha in non-small cell lung cancer. *Cancer Res.* 2006; 66:143-50.
57. Farrand L, Byun S, Kim JY, Im-Aram A, Lee J, Lim S, et al. Piceatannol enhances cisplatin sensitivity in ovarian cancer via modulation of p53, X-linked inhibitor of apoptosis protein (XIAP), and mitochondrial fission. *J Biol Chem.* 2013; 288:23740-50.
58. Greenhough A, Smartt HJ, Moore AE, Roberts HR, Williams AC, Paraskeva C, et al. The COX-2/PGE2 pathway: key roles in the hallmarks of cancer and adaptation to the tumour microenvironment. *Carcinogenesis.* 2009; 30:377-86.
59. Zhou J, Li G, Zheng Y, Shen H-M, Hu X, Ming Q-L, et al. A novel autophagy/mitophagy inhibitor liensinine sensitizes breast cancer cells to chemotherapy through DNMI1L-mediated mitochondrial fission. *Autophagy.* 2015; 11:1259-79.
60. Zhang N, Yin Y, Xu S-J and Chen W-S. 5-Fluorouracil: mechanisms of resistance and reversal strategies. *Molecules.* 2008; 13:1551-69.
61. Ghosh N, Chaki R, Mandal V and Mandal SC. COX-2 as a target for cancer chemotherapy. *Pharmacol Rep.* 2010; 62:233-44.
62. Cronin-Fenton DP, Heide-Jorgensen U, Ahern TP, Lash TL, Christiansen P, Ejlersten B, et al. Low-dose Aspirin, nonsteroidal anti-inflammatory drugs, selective COX-2 inhibitors and breast cancer recurrence. *Epidemiology.* 2016; 27:586-93.
63. Thun MJ, Henley SJ and Patrono C. Nonsteroidal anti-inflammatory drugs as anticancer agents: mechanistic, pharmacologic, and clinical issues. *J Natl Cancer Inst.* 2002; 94:252-66.
64. Wang Q, Zhang M, Torres G, Wu S, Ouyang C, Xie Z, et al. Metformin suppresses diabetes-accelerated atherosclerosis via the inhibition of Drp1-mediated mitochondrial fission. *Diabetes.* 2017; 66:193-205.
65. Li A, Zhang S, Li J, Liu K, Huang F and Liu B. Metformin and resveratrol inhibit Drp1-mediated mitochondrial fission and prevent ER stress-associated NLRP3 inflammasome activation in the adipose tissue of diabetic mice. *Mol Cell Endocrinol.* 2016; 434:36-47.
66. Yu X, Mao W, Zhai Y, Tong C, Liu M, Ma L, et al. Anti-tumor activity of metformin: from metabolic and epigenetic perspectives. *Oncotarget.* 2017;8(3):5619-28.
67. Qian W, Wang J, Roginskaya V, McDermott LA, Edwards RP, Stolz DB, et al. Novel combination of mitochondrial division inhibitor 1 (mdivi-1) and platinum agents produces synergistic pro-apoptotic effect in drug resistant tumor cells. *Oncotarget.* 2014; 5:4180-94.
68. Xu S, Pi H, Zhang L, Zhang N, Li Y, Zhang H, et al. Melatonin prevents abnormal mitochondrial dynamics resulting from the neurotoxicity of cadmium by blocking calcium-dependent translocation of Drp1 to the mitochondria. *J Pineal Res.* 2016; 60:291-302.
69. Wu H, Wang Y, Wu C, Yang P, Li H and Li Z. Resveratrol induces cancer cell apoptosis through MiR-326/PKM2-mediated ER stress and mitochondrial fission. *J Agric Food Chem.* 2016; 64:9356-67.
70. Shamsara J and Shahr-Sadr A. Developing a CoMSIA model for inhibition of COX-2 by resveratrol derivatives. *Iran J Pharm Res.* 2016; 15:459-69.
71. Bishayee A. Cancer prevention and treatment with resveratrol: from rodent studies to clinical trials. *Cancer Prev Res.* 2009; 2:409-18.